CDCP1 controls compensatory renal growth by integrating Src and Met signaling

Kentaro Kajiwara[1*], Kazuhiro Aoki[2], Daisuke Okuzaki[3], Kunio Matsumoto[4] and Masato Okada[1*]

[1] Department of Oncogene Research, Research Institute for Microbial Diseases, Osaka University, Osaka 565-0871, Japan

[2] Division of Quantitative Biology, Okazaki Institute for Integrative Bioscience, National Institute for Basic Biology, National Institutes of Natural Sciences, Aichi 444-8787, Japan

[3] Genome Information Research Center, Research Institute for Microbial Diseases, Osaka University, Osaka 565-0871, Japan

[4] Division of Tumor Dynamics and Regulation, Cancer Research Institute, Kanazawa University, Ishikawa 920-1192, Japan

* Corresponding authors: Masato Okada and Kentaro Kajiwara.
Email: okadam@biken.osaka-u.ac.jp, kajiwara@biken.osaka-u.ac.jp.

Running title: CDCP1 controls HGF-induced renal growth

Abstract

Compensatory growth of organs after loss of mass and/or function is controlled by hepatocyte growth factor (HGF), but the underlying regulatory mechanisms remain elusive. Here, we show that the transmembrane glycoprotein CUB domain-containing protein 1 (CDCP1) controls compensatory renal growth by acting as a critical regulator of HGF signaling. In MDCK cysts, HGF induces the temporal upregulation of Src and its scaffold CDCP1, and the ablation of CDCP1 abrogates HGF-induced morphological change and cell growth. Mechanistically, upregulated CDCP1 recruits Src into lipid rafts to activate STAT3 associated with the HGF receptor Met, resulting in the upregulation of downstream factors required for HGF functions. *In vivo,* CDCP1 is upregulated in the renal tubules after unilateral nephrectomy, and the ablation of CDCP1 significantly suppresses compensatory renal growth by attenuating Met-STAT3 signaling. These findings demonstrate that CDCP1 controls HGF-induced compensatory renal growth by integrating Src and Met signaling, and provide new insights into the regulatory mechanisms underlying the multifaceted functions of HGF during regenerative growth of various organs.

Key words: compensatory growth/HGF/lipid rafts/MDCK cells/STAT3

Introduction

Controlling of organ size during development and/or regenerative growth is important to maintain organ function, body homeostasis, and health. The kidneys are paired organs that generate urine through the filtration of blood and reabsorption of water and nutrients, and kidney mass is strictly related to total body mass. The renal tubules constitute most of the mass and function, and have a remarkable capacity to undergo regenerative growth. Unilateral nephrectomy (UNX), a surgical procedure to reduce kidney mass, increases fluid flow in the remaining kidney and promotes the subsequent growth and proliferation of tubular epithelial cells to compensate for the increased flow (Fine, 1986). This compensatory renal growth is regulated via the activation of mTOR signaling pathways (Chen et al, 2005; Chen et al, 2009; Chen et al, 2015). However, interfering with the function of this pathway does not completely suppress renal growth, suggesting the potential contribution of one or more additional signaling pathways.

Compensatory renal growth also requires a number of growth factors (Hammerman et al, 1993), among which hepatocyte growth factor (HGF) plays a prominent role (Trusolino et al, 2010). HGF is produced by the surrounding or distal mesenchyme in the remaining kidney immediately after UNX (Ishibashi et al, 1992; Joannidis et al, 1994; Nagaike et al, 1991), inducing the upregulation of its receptor, Met, in the renal tubules (Ishibashi et al, 1992). In addition, HGF promotes dynamic morphogenesis through the induction of epithelial-mesenchymal transition (EMT) in epithelial cells during development and regenerative growth of the kidney (Chang-Panesso & Humphreys, 2017; Matsumoto & Nakamura, 2001). HGF-mediated morphogenesis requires STAT3 signaling (Boccaccio et al, 1998), which is regulated by Met through endosomal trafficking (Kermorgant & Parker, 2008). However, the molecular mechanisms through which the multifaceted HGF functions are precisely controlled during compensatory renal growth remain elusive.

Madin-Darby Canine Kidney (MDCK) cell-line was derived from renal tubule epithelial cells and is a physiologically relevant *in vitro* model to study the regulation of HGF functions in the kidney (O'Brien et al, 2002; Zegers, 2014). When grown in three-dimensional cultures, MDCK cells spontaneously form spherical cysts that resemble renal tubules, comprising an epithelial monolayer and lumen. Upon stimulation with HGF, MDCK cysts undergo morphological alterations and form branched tubular structures (Montesano et al, 1991a; Montesano et al, 1991b). During this morphogenesis, MDCK cells lose their epithelial polarity via a partial EMT-like phenotypic change, and protrude into the extracellular matrix (ECM) by penetrating the basement membrane (O'Brien et al, 2004; Pollack et al, 1998). In addition, HGF promotes cell growth and proliferation, resulting in the formation of multi-cell layered cysts. To elucidate the mechanisms underlying HGF-induced phenotypic changes, the roles of multiple signaling axes downstream of Met, such as the Ras-ERK, Akt-mTOR, Src, and STAT3 pathways, have been investigated extensively (Khwaja et al, 1998; Nakamura et al, 2011; O'Brien et al, 2004; Pollack et al, 1998; Santos et al, 1993). However, the molecular mechanism by which these diverse signaling pathways are accurately coordinated by HGF–Met needs to be clarified. Furthermore, the most critical pathway for HGF-induced compensatory renal growth remains undefined.

Here, using three-dimensional cultures of MDCK cysts as a model of renal tubules, we identified Src and its membrane scaffold, CUB domain-containing protein 1 (CDCP1), as critical elements of HGF signaling. We then investigated the mechanisms underlying the functions of the CDCP1–Src axis in MDCK cysts and verified its physiological roles in compensatory renal growth using *Cdcp1*-knockout mice. The results obtained in these studies demonstrate that CDCP1 plays a crucial role in controlling HGF-induced compensatory renal growth by focally and temporally integrating Src and Met-STAT3 signaling on lipid rafts.

Results

CDCP1 is required for HGF signaling in MDCK cysts

MDCK cells cultured in a collagen matrix formed cyst structures with a luminal space (**Fig 1A**). HGF treatment immediately promoted cell growth/proliferation (as indicated by increased cyst diameter) and morphological changes with some cysts exhibiting extended cell

protrusions (Gao & Vande Woude, 2005; O'Brien et al, 2002) (**Fig 1, A–C**). Similar HGF-induced effects were observed in primary cultured renal proximal tubule cells (Bowes et al, 1999), indicating that MDCK cysts are suitable for the mechanistic analysis of HGF functions. To dissect the HGF-related signaling pathways, we first examined the effects of various signaling inhibitors on HGF-induced phenomena. Treatment of MDCK cysts with NK4, a specific HGF antagonist (Date et al, 1997), robustly inhibited cell proliferation and morphological changes, confirming that the observed phenomena were dependent on HGF. Treatment of the cysts with Torin1 or rapamycin, selective mTOR inhibitors, significantly suppressed cell growth/proliferation but was less effective against the formation of cell protrusions (**Fig 1, A–C**). By contrast, treatment with dasatinib, a Src kinase inhibitor, potently suppressed both cell proliferation and protrusion extension (**Fig 1, A–C**). Furthermore, an immunofluorescence analysis revealed that activated Src (pY418) was concentrated at the tip of protruding cells (**Fig 1D**) and co-localized with mCherry-GPI, a marker protein of lipid rafts (**Fig 1E**). These observations imply that HGF signaling is associated with the activation of Src in lipid rafts on protruding cells.

To assess its role in HGF signaling further, we examined the effects of Src activation on MDCK cells by expressing Src-MER, a Src protein fused to a modified estrogen receptor (MER) (Kuroiwa et al, 2011) that could be activated by treatment with hydroxytamoxifen (4-OHT) (**Fig EV1A**). Src activation induced both the formation of multiple cell protrusions and cell proliferation (**Fig EV1B**), supporting the involvement of Src activity in HGF signaling. A detergent-resistant membrane (DRM) separation analysis revealed that activated Src-MER was concentrated in lipid raft fractions (**Fig EV1C**). Because Src alone can only partially localize to lipid rafts (Oneyama et al, 2009), we searched for scaffolding proteins that accommodate and activate Src in these structures. Src-MER interacting proteins were isolated from DRM fractions by co-immunoprecipitation and identified by mass spectrometry (**Fig EV1, D and E**). Among the candidate proteins identified, we selected the transmembrane glycoprotein CDCP1 for further analysis because it has palmitoylation sites required for lipid raft localization and serves as a membrane adaptor of Src (Alvares et al, 2008; Wortmann et al, 2009) (**Fig EV2A**). We then validated the roles of CDCP1 in HGF signaling. An immunofluorescence analysis revealed that endogenous CDCP1 was transiently concentrated at the tips of protruding cells during the early stage of morphological changes (**Fig 1F**), in a manner similar to that of activated Src and mCherry-GPI (**Fig 1, D and E**). More importantly, HGF-induced cell protrusion extension and cell proliferation were efficiently abrogated by *Cdcp1*-knockout in MDCK cells (**Fig 1, G–I and Fig S2, B–D**). These results suggest that the CDCP1-Src axis is a crucial component of HGF signaling.

Upregulation of CDCP1 induces HGF-related phenotypic changes by activating Src in lipid rafts

To elucidate the mechanisms through which CDCP1 regulates HGF signaling, we generated MDCK cells in which the expression of CDCP1-EGFP could be controlled by doxycycline (Dox). Dox treatment induced the expression of full-length and cleaved CDCP1 at the plasma membrane (**Fig EV3, A and B**). A DRM separation analysis showed that a fraction of CDCP1 was distributed in lipid raft-enriched fractions (**Fig EV3C**). Moreover, the induction of CDCP1 expression dramatically increased the amount of phosphorylated Src (pY418) without affecting Src protein levels (**Fig EV3A**), indicating that Src was activated by the upregulation of CDCP1. Furthermore, activated Src was concentrated in the lipid raft fractions and was physically associated with CDCP1 (**Fig EV3, C and D**). By contrast, a CDCP1 mutant that lacked the Src-binding site (Y734F; CDCP1-YF) failed to activate Src (**Fig EV3A**). A different CDCP1 mutant lacking the lipid raft localization signal (C689G–C690G; CDCP1-CG) was able to activate Src, but only in non-lipid raft fractions (**Fig EV3, A and C**). These findings corroborate the notion that CDCP1 specifically activates Src in lipid rafts.

Next, we examined the effects of CDCP1 expression on the phenotypes of MDCK cysts (**Fig 2A**). CDCP1 expression was induced after the completion of cystogenesis and morphological changes were observed (**Movie EV1**). In the early stages (12–24 h after induction), cells expressing CDCP1 gradually protruded toward the ECM. During the later stages (48 h after induction), multiple cell protrusions formed randomly and extended

aggressively toward the ECM, with cysts forming multiple layers (**Fig 2B**). Concurrent with these phenomena, upregulation of CDCP1 activated Src in the protruding cells (**Fig 2C**), and inhibition of Src by dasatinib strongly suppressed CDCP1-induced cell proliferation and protrusion extension (**Fig 2D and Table EV1**). Meanwhile, the upregulation of CDCP1-YF or CDCP1-CG did not significantly induce phenotypic changes (**Fig 2, E and F**). Based on these results, it is likely that upregulation of CDCP1 can induce HGF-related phenotypic changes, i.e., cell protrusion formation and cell proliferation, in MDCK cysts via the activation of Src in lipid rafts.

CDCP1 activates the STAT3 pathway via lipid rafts

To dissect the signaling pathways downstream of the CDCP1–Src axis, we performed DNA microarray analyses of MDCK cysts expressing either wild-type CDCP1 or the CDCP1-CG mutant. A gene ontology analysis implied that CDCP1 expression is involved in the regulation of signal transduction (**Fig EV4A**) and Ingenuity Pathway Analysis revealed that the STAT3 pathway was more prominently activated by CDCP1 expression than by CDCP1-CG expression (**Fig EV4, B and C, Dataset EV1**). Indeed, the level of phosphorylated STAT3 (pY705) increased significantly in cysts expressing wild-type CDCP1 (**Fig 3A**). STAT3 is a transcription factor that is activated by Src-mediated phosphorylation of Tyr705 (Bromberg et al, 1998) and regulates various cellular events including the upregulation of MMPs (Yu et al, 2009) and mitogenic genes.

A qPCR analysis confirmed that the expression levels of several matrix metalloproteinase (MMP)-encoding genes were significantly increased by upregulation of CDCP1 (**Fig 3B**). In addition, immunofluorescent staining of laminin revealed that CDCP1 expression disrupted the basement membrane, allowing the extension of cell protrusions (**Fig EV5A**). This effect was suppressed by treatment with marimastat, a pan-MMP inhibitor (**Fig EV5, B and C**). Similar suppression of cell protrusion extension by marimastat was also observed in HGF-stimulated MDCK cysts (**Fig EV5, D and E**). Analysis with DQ-collagen, a fluorescent indicator of collagen degradation, also showed that CDCP1 expression induced degradation of the ECM (**Fig EV5F**). These observations suggest that the HGF-induced formation of cell protrusions is associated with ECM rearrangements via STAT3-induced upregulation of MMPs. The expression of mitogenic genes such as *Myc* (Myc) and *Ccnd1* (Cyclin D1) was also upregulated in cysts expressing CDCP1 (**Fig 3B**), indicating that CDCP1-induced cell proliferation is attributable to STAT3 activation.

We confirmed the contribution of STAT3 to cell protrusion formation and proliferation by specifically perturbing its activity. Activation of STAT3 using the STAT3-MER system induced the formation of cell protrusions and a multi-layered structure (**Fig EV5G**). By contrast, treatment of MDCK cysts with STAT3-specific inhibitors suppressed CDCP1-induced cell growth (**Fig 3C and Table EV1**), and overexpression of dominant negative STAT3 (STAT3-Y705F) also inhibited CDCP1-induced cellular events (**Fig 3D**). Furthermore, STAT3 inhibitors efficiently suppressed cell protrusion formation (**Fig 3E**) and proliferation (**Fig 3F**) in HGF-stimulated MDCK cysts, underscoring the crucial role of STAT3 activation in HGF functions.

CDCP1 focally integrates Src and Met-STAT3 signaling

Next, we investigated the functional link between the HGF-Met pathway and the CDCP1-Src axis. An inhibitor screening assay showed that various Met-specific inhibitors potently suppressed CDCP1-induced phenotypic changes (**Fig 4A and Table EV1**), suggesting that Met activity is involved in the function of CDCP1. Because activated Met associates with STAT3, we predicted a close association between CDCP1-Src and Met-STAT3. To assess physical interactions between these proteins, Met and various CDCP1 mutants that lacked particular extracellular CUB domains were co-expressed in HEK293 cells (**Fig 4, B and C**). Co-immunoprecipitation assays revealed that CDCP1 interacted with Met. This interaction was enhanced by removal of the first CUB domain of CDCP1 but diminished by deletion of all CUB domains (**Fig 4, B and C**), indicating that CDCP1 interacts with Met through extracellular domains, and that removal of the first CDCP1 CUB domain is required for efficient association with Met.

Because CDCP1 is activated via proteolytic shedding between the first and second CUB domains (Casar et al, 2012; He et al, 2016), it is likely that activated CDCP1 functionally interacts with Met. To verify this hypothesis, we analyzed the function of a mutant CDCP1 (CDCP1-PR) rendered resistant to proteolytic shedding due to the presence of three point mutations within the protease recognition sites (K365A-R368A-K369A) (**Fig 4D**). Expression of CDCP1-PR induced the activation of Src to a level similar to that observed with wild-type CDCP1 but failed to activate STAT3 (**Fig 4D**). Consistent with these biochemical effects, of CDCP1-PR failed to induce the formation of cell protrusions (**Fig 4, E and F**). These data suggest that an association between cleaved CDCP1 and Met is required for Src-mediated STAT3 activation and subsequent cellular events (**Fig 4G**). The functional interaction between Met and CDCP1 was further confirmed using *Cdcp1*-knockout MDCK cysts. The initiation of cell protrusion induced by HGF treatment or overexpression of Met was efficiently suppressed by the loss of CDCP1 (**Fig EV6A**). Taken together, these lines of *in vitro* evidence suggest a model in which the upregulation of CDCP1-Src in lipid rafts is required for Met-mediated STAT3 activation during HGF-induced phenotypic changes (**Fig EV6B**).

Compensatory renal growth is suppressed in Cdcp1-knockout mice

To verify the aforementioned model *in vivo*, we investigated the role of the CDCP1-mediated Met-STAT3 pathway in compensatory renal growth following UNX. For this *in vivo* study, we generated Cdcp1-knockout mice in a C57/BL6 background using the CRISPR-Cas9 system (**Fig EV7, A–C**). The Cdcp1-knockout (*Cdcp1*$^{-/-}$) mice grew normally and did not show any overt phenotype under normal conditions (**Fig EV7, C–E**), as reported previously (Spassov et al, 2013). Eight weeks after UNX, the remaining kidney was enlarged in wild-type and heterozygous (*Cdcp1*$^{+/-}$) mice (**Fig 5A**). Kidney/body weight ratios in wild-type and *Cdcp1*$^{+/-}$ mice were elevated to approximately 136% and 135% relative to those in sham-operated mice, respectively. By contrast, the kidney/body weight ratio elevation was significantly smaller in *Cdcp1*$^{-/-}$ mice (approximately 121%) (**Fig 5B**). Since compensatory renal growth is achieved via the expansion of proximal renal tubules (Anderson, 1967; Chen et al, 2015), we visualized the renal tubules using a fluorescein-labeled specific lectin (LTL-FITC). Wild-type mice exhibited prominent thickening of LTL-positive proximal renal tubules (to approximately 148%), whereas this thickening was suppressed in *Cdcp1*$^{-/-}$ mice (approximately 117%) (**Fig 5, C and D**). These data were consistent with the observed elevation of the kidney/body weight ratios (**Fig 5B**), confirming that compensatory growth of proximal renal tubules is suppressed in *Cdcp1*$^{-/-}$ mice.

Met-STAT3 signaling is attenuated in *Cdcp1*-knockout mice

To address the cause of defective renal growth in *Cdcp1*$^{-/-}$ mice, we analyzed the remaining kidney at earlier stages of compensatory growth (within 4 days after UNX) because the expression of HGF and Met is transiently upregulated in renal tissues within 12 h (Ishibashi et al, 1992; Nagaike et al, 1991). The mass of the remaining kidney immediately increased in wild-type mice (**Fig 6A**), whereas acute enlargement of the kidney tended to be delayed in *Cdcp1*$^{-/-}$ mice. Immunofluorescence analysis revealed that activation of Met (pY1234/1235) and STAT3 (pY705) occurred in wild-type renal tubules 12 h after UNX, as reported previously (Kermorgant & Parker, 2008), while the activation of both signals was appreciably attenuated in *Cdcp1*$^{-/-}$ renal tubules (**Fig 6, B and C**). Activation of CDCP1 (pY734) also ocurred in renal tubules in a manner similar to that of Met and STAT3 (**Fig EV8A**). Notably, activated Met, STAT3, and CDCP1/Src were co-localized in a subset of intracellular small vesicles that were positive for EEA1 (**Fig EV8, B–D**), a marker of early endosomes, supporting the intimate interactions among these signaling molecules. These results suggest that the CDCP1-Src axis mediates HGF-Met-STAT3 signaling even in proximal renal tubules.

We also analyzed cell proliferation by immunostaining for Ki67. The ratios of Ki67-positive cells in wild-type proximal tubules were gradually elevated and peaked 2 days after UNX (**Fig 6, D and E**). However, in *Cdcp1*$^{-/-}$ mice, the appearance of Ki67-positive cells was delayed, and the overall number of proliferating cells was decreased. These results suggest that HGF-induced cell proliferation through Met-STAT3 signaling is also attenuated in *Cdcp1*$^{-/-}$ mice, thereby retarding the onset of compensatory renal growth.

Finally, we examined the effects of CDCP1 loss on the surrounding environment of proximal tubules after UNX. Proximal tubules are covered by a basement membrane comprised mainly of collagen IV. Before UNX, collagen IV was observed around the proximal tubules in both wild-type and *Cdcp1*$^{-/-}$ mice (**Fig 6F**). In wild-type mice, collagen IV was gradually degraded 24 h after UNX, but this degradation was attenuated in *Cdcp1*$^{-/-}$ mice. To identify the molecules involved in basement membrane degradation, we focused our analysis on secretory MMPs, including MMP2 and MMP9, both of which are targets of STAT3 and are expressed in proximal tubules (Tan & Liu, 2012). In wild-type mice, MMP2 and MMP9 were upregulated and occasionally concentrated in vesicle-like structures in proximal tubules 24 h after UNX (**Fig 6G and Fig EV8E**). However, these phenomena were barely detectable in *Cdcp1*$^{-/-}$ proximal tubules. These observations suggest that secretory MMPs contribute to compensatory renal growth downstream of CDCP1-Src-mediated Met-STAT3 signaling.

Discussion

To address the regulatory mechanisms underlying HGF-induced regenerative renal growth, we dissected the HGF signaling using MDCK cysts as a model of renal tubules, and identified Src and its scaffold CDCP1 as critical elements of HGF signaling. Upon stimulation with HGF, CDCP1 was temporally concentrated at the tip of protruding cells. Since previous reports showed that CDCP1 expression is induced by HGF (Gusenbauer et al, 2013) or by epidermal growth factor (EGF)-mediated activation of the MAPK pathway (Adams et al, 2015; Dong et al, 2012), it is likely that the observed upregulation of CDCP1 was caused by activation of the HGF-Met-MAPK pathway. We also found that continuous upregulation of CDCP1 induced the formation of multiple cell protrusions and cell growth/proliferation. Notably, when CDCP1 expression was halted by removing Dox from the media, cells in the protruding cord-like structures recovered epithelial features, resulting in the formation of a luminal structure (**Fig EV9A**). This finding suggests that the temporal upregulation of CDCP1 by growth factors such as HGF might trigger the initial phase of morphogenesis, specifically cell protrusion extension and growth, and that the coordinated negative feedback regulation of CDCP1 might be involved in establishing the compound tubular/acinar epithelial system.

In our model system, CDCP1 was tyrosine-phosphorylated by Src, and trapped and further activated Src particularly in lipid rafts. Although CDCP1-mediated Src activation has been reported in other cell types (Liu et al, 2011; Wortmann et al, 2011), we demonstrated here that localization of the CDCP1–Src complex in lipid rafts is required for HGF-induced phenotypic changes in MDCK cysts. We also found that upregulation of CDCP1 focally activates Src in lipid rafts to induce the phosphorylation of STAT3 at Tyr705 (Bromberg et al, 1998; Yu et al, 1995). Furthermore, activated STAT3 induced the upregulation of MMPs and mitogenic factors such as Myc and Cyclin D1, which promote cell protrusion extension and cell proliferation, respectively. These findings suggest that the activation of STAT3 via CDCP1-Src is one of the major pathways involved in HGF signaling. We also found that a physical association between cleaved/activated CDCP1 and Met is required for STAT3 activation. Because STAT3 interacts directly with activated Met through an SH2 domain (Boccaccio et al, 1998), it is likely that the cleaved form of CDCP1 binds Src and interacts with the Met-STAT3 complex in lipid rafts to allow the efficient phosphorylation of STAT3 by Src (**Fig 4G**). This focal integration of the CDCP1-Src axis with the Met-STAT3 complex in lipid rafts might be crucial for the activation of STAT3 that is required for HGF function. CDCP1 can also interact with other transmembrane receptors, including HER2, EGFR, integrin β1 and E-cadherin (Alajati et al, 2015; Casar et al, 2014; Law et al, 2013; Law et al, 2016). For example, HER2 associates stably with CDCP1 and forms a heterodimer complex on the plasma membrane; this interaction enhances Src activity in an EGF-independent manner (Alajati et al, 2015). Together with our results presented here, these previous findings indicate that CDCP1 is a more general regulator of membrane receptor signaling, which involves Src activation.

Upregulation of CDCP1 has been implicated in tumor progression (Alajati et al, 2015; Awakura et al, 2008; Dong et al, 2012; Emerling et al, 2013; He et al, 2016; Hooper et al, 2003; Ikeda et al, 2009; Leroy et al, 2015; Miyazawa et al, 2010; Scherl-Mostageer et al, 2001; Turdo et al, 2016; Wright et al, 2016). In some cancer cells, upregulated CDCP1 promotes invasion, metastasis, and tumor growth (Alajati et al, 2015; Casar et al, 2012;

Kollmorgen et al, 2013; Lin et al, 2014; Liu et al, 2011; Miyazawa et al, 2010; Turdo et al, 2016; Uekita et al, 2007), although the underlying mechanisms remain elusive. Our findings presented here suggest that CDCP1-mediated activation of the Src-STAT3 pathway contributes to malignant progression by inducing invasive and growth promoting phenotypes, even in cancer cells. Indeed, we found that upregulation of CDCP1in MDCK cysts induced the expression of cytokeratin 14 (**Fig EV9B**), a promising marker of collective cancer invasion (Cheung et al, 2013), suggesting a potential role of upregulation of the CDCP1-Src axis in this process. Further analyses of the functions of the CDCP1–Src–Met–STAT3 pathway in a wide range of cancer cells could reveal new therapeutic targets for the treatment of some malignant cancers.

HGF is immediately upregulated after the loss of kidney mass and plays important roles in compensatory growth through the induction of cell proliferation and anti-apoptotic effects (Matsumoto & Nakamura, 2001). In this study, we uncovered the contribution of CDCP1-Src to HGF-induced compensatory renal growth using Cdcp1-deficient mice. Immunofluorescence analyses showed that activation of Met and STAT3 in the renal tubule cells following UNX was significantly attenuated in Cdcp1-deficient mice. Furthermore, upregulation of MMP2/9 and degradation of basement membrane collagen IV (Tan & Liu, 2012) were detected in the renal tubule cells after UNX (**Fig EV8F**). These observations are consistent with those of our *in vitro* study of MDCK cysts, supporting the crucial role of the functional integration of CDCP1-Src with Met-STAT3 pathways, even during compensatory renal growth. However, the renal growth was not completely suppressed by CDCP1 loss, suggesting that some other CDCP1-related molecules or distinct growth factor signaling pathways might compensate for the function of CDCP1 *in vivo*. Given that the expression of CDCP1 is temporally upregulated under pathological conditions such as tissue injury, hypoxia, and cancer recurrence (He et al, 2016), it is likely that upregulated CDCP1 might function to acutely amplify the HGF signaling that is required for regenerative organ growth in critical situations. Furthermore, since STAT3 is an important regulator of the regeneration of other organs such as the liver, intestine, and muscle (Lindemans et al, 2015; Taub, 2004; Tierney et al, 2014), it is also possible that the temporal upregulation of CDCP1 contributes more strongly to the promotion of organ regeneration by inducing focal activation of the Src-STAT3 pathway.

In conclusion, we found that CDCP1 serves as a critical regulator of HGF-induced compensatory renal growth by focally integrating Src and the Met-STAT3 pathway (**Fig 6H**). Our discovery of the CDCP1-Src axis as a new component of HGF-Met signaling provides insights into the regulatory mechanisms underlying the multifaceted functions of HGF during morphogenesis and/or regenerative growth, and might contribute to the development of more promising therapies for malignant cancers that are associated with the upregulation of CDCP1 and Met.

Materials and Methods

Cell culture

MDCK type I and HEK293T cells were cultured in DMEM supplemented with 10% foetal bovine serum (FBS) at 37 °C in a 5% CO_2 atmosphere. Three-dimensional culture was performed using collagen type I (Cellmatrix Type I-A, Nitta Gelatin) according to the manufacturer's protocol. Collagen type I-A (3 mg/ml) was neutralised with reconstitution buffer (2.2% $NaHCO_3$, 0.05 N NaOH and 200 mM HEPES) and diluted with 5× DMEM (Gibco). MDCK cells (1.5×10^5 cells/ml of the collagen gel) were combined with the collagen in DMEM supplemented with 5% FBS, and then polymerised at 37 °C in a 5% CO_2 atmosphere. The medium was replaced every 2 days. For the DQ-collagen degradation assay, a collagen gel containing 2% DQ-collagen type I (Molecular Probes) was used.

Mice

Cdcp1-knockout mice were generated in a C57BL/6N using the CRISPR/Cas9 system. Animals were housed in environmentally controlled rooms at the animal experimentation facility at Osaka University. All animal experiments were carried out according to the guidelines of the Osaka University committee for animal and recombinant DNA experiments

and were approved by the Osaka University Institutional Review Board. The sequence of gRNA and primers used in genotyping are listed in Supplementary Table 3 (see also Supplementary Fig. 9a).

Antibodies and inhibitors

The following primary antibodies were used in this study: anti-CDCP1 (4115), anti-CDCP1 pY734 (9050), anti-STAT3 (9132), anti-STAT3 pY705 (9145), anti-myc-tag (2276), anti-Met pY1234/1235 (3077), and anti-Met (8198) antibodies were all purchased from Cell Signaling Technologies), anti-CDCP1 antibody (LC-C172540) was purchased from LSBio, anti-SFK (sc-18, clone SRC2), anti-ERα (sc-542, clone MC-20), anti-Gapdh (sc-32233, clone 6C5), and anti-MMP2 (sc-10736) antibodies were all purchased from Santa Cruz Biotechnology, anti-Src pY418 (44-655G), anti-Src pY529 (44-662G), and anti-Ki67 (14-5698-82) antibodies were all purchased from Thermo Fisher Scientific, anti-Src (OP07, clone Ab-1), anti-phosphotyrosine (05-1050, clone 4G10), and anti-MMP9 (444236) antibodies were all purchased from Millipore, anti-collagen IV antibody (ab6586) was purchased from abcam, anti-laminin antibody (L9393) was purchased from Sigma, and anti-keratin 14 antibody (PRB-155P, clone AF64) was purchased from Covance. The following inhibitors were used in this study: S3i-201 (573102), Stattic (573099), JAK inhibitor 1 (420099), c-Met/Ron dual kinase inhibitor (448104), and Rac1 inhibitor (553502) were purchased from Calbiochem, Marimastat (M2699) was purchased from Sigma, Y27632 (257-00511) from Wako, and other inhibitors listed in Supplementary Table 1 were all purchased from the Screening Committee of Anticancer Drugs.

Immunoblotting and immunoprecipitation

For two-dimensional culture, cells were lysed in n-octyl-β-D-glucoside (ODG) buffer [20 mM Tris-HCl (pH 7.4), 150 mM NaCl, 1 mM EDTA, 1 mM Na_3VO_4, 20 mM NaF, 1% Nonidet P-40, 5% glycerol, 2% ODG and a protease inhibitor cocktail (Nacalai Tesque)], and immunoblotting was performed. For three-dimensional culture, the cyst-containing collagen matrix was incubated with HBS buffer [10 mM HEPES (pH 7.3), 140 mM NaCl, 4 mM KCl, 1.8 mM $CaCl_2$ and 1 mM $MgCl_2$] containing 0.1% collagenase (Roche) at 37 °C. Cysts were harvested by centrifugation and lysed in SDS sample buffer [50 mM Tris-HCl (pH 6.8), 2% SDS, 100 mM NaCl, 1 mM EDTA, 1 mM Na_3VO_4, 20 mM NaF and 5% sucrose] before immunoblotting. For immunoprecipitation assays, cells were lysed in ODG buffer and the lysates were incubated with an anti-myc-tag antibody (2276, Cell Signaling Technology). Immunoprecipitated proteins were pulled down with protein A-sepharose (GE Healthcare) for immunoblotting. Horseradish peroxidase (HRP)-conjugated anti-mouse or anti-rabbit IgG (Zymed) was used as the secondary antibody. All immunoblots were visualised and quantitated using a Luminograph II System (Atto). Silver staining was performed using the Silver Stain MS Kit (Wako).

DRM fractionation

Cells were lysed in homogenisation buffer [50 mM Tris-HCl (pH 7.4), 150 mM NaCl, 1 mM EDTA, 1 mM Na_3VO_4, 20 mM NaF, 0.25% Triton X-100 and protease inhibitor cocktail] and separated on a discontinuous sucrose gradient (5–35–40%) by ultracentrifugation at 150,000 × *g* for 12 h at 4 °C using an Optima L-100XP centrifuge equipped with a SW55Ti rotor (Beckman Coulter). The 11 fractions were collected from the top of the sucrose gradient.

Microarray analysis and quantitative real-time PCR

For microarray analysis, total RNA was isolated from MDCK cysts using the Sepasol-RNA Kit (Nacalai Tesque). Microarray analysis was performed on a G2505C Microarray Scanner (Agilent Technologies) using the Canis (V2) Gene Expression Microarray 4×44K (Agilent Technologies). Microarray data were subjected to gene ontology analysis and upstream regulator analysis using the IPA Program (Qiagen, http://www.qiagenbioinfomatics.com/). For quantitative real-time PCR analysis, cDNA was prepared from RNA using the Transcriptor First Strand cDNA Synthesis Kit (Roche) according to the manufacturer's instructions. Real-time PCR was performed on a 7900HT Fast Real-Time PCR System (Applied Biosystems) using the Thunderbird qPCR Mix (Toyobo). Total RNA was normalised to expression of the housekeeping gene GAPDH. The primers used in this analysis are listed in **Table EV2**.

Immunofluorescent microscopy

For two-dimensional culture, cells were grown on collagen type I-coated coverslips, fixed with 4% paraformaldehyde and then permeabilized with PBS containing 0.03% Triton X-100. For three-dimensional culture, cysts embedded within the collagen matrix were fixed with 4% paraformaldehyde and permeabilized with PBS containing 0.5% Triton X-100. Permeabilized cells and cysts were blocked with 1% BSA and incubated with primary antibodies, and then incubated with Alexa Fluor 488/594-phalloidin (Molecular Probes). For the kidney sections, kidneys were prepared from perfusion fixation with 4% paraformaldehyde and dissected. The fixed kidneys were embedded in OCT compound (Sakura Finetek), sectioned, and mounted on glass slides. The kidney sections were blocked with Blocking One (Nacalai Tesque), incubated with primary antibodies, and then incubated with Alexa Fluor 488/594-conjugated secondary antibodies (Molecular Probes) and the fluorescein-conjugated proximal tubule marker, FITC-LTL (FL-1321, Vector Laboratories). Nuclei were counterstained with DAPI. Immunostained objects were observed under a FV1000 confocal microscope (Olympus). For time-lapse observation of three-dimensional cultures, cysts embedded within in collagen matrix were observed under a FV1200 confocal microscope (Olympus).

CRISPR/Cas9-based generation of *CDCP1*-knockout MDCK cells

Target-gRNA containing the pSilencer1.0-U6 plasmid, Cas9 and the EGFP co-expressing plasmid (pMJ920; Addgene) were transfected into MDCK cells with MDCK Cell Avalanche Transfection Reagent according to the manufacturer's protocol (EZ Bioscience). Three days after transfection, EGFP-positive single cells were isolated with a FACSAria III Sorter (BD Biosciences). Knockout of the *Canis CDCP1* gene was confirmed by immunoblotting. The sequence of the gRNA and the primers used in genotyping are listed in **Table EV3** (see also **Fig EV2B**).

Plasmid construction and gene transfer

CDCP1, CDCP1 deletion mutants, STAT3, and Met were generated by PCR using human cDNA as the template and subcloned into the pCX4 retroviral plasmid (generously donated by Dr. Akagi) (Akagi et al, 2003). CDCP1 mutants (K365A-R368A-K369A, C689G-C690G and Y734F) and STAT3-Y705F were generated by mutagenesis PCR using KOD-Plus polymerase (Toyobo). CDCP1 and its respective mutants were subcloned into either pEGFP-N1 or pmCherry-N1 plasmid (Clontech), and then further subcloned into the pRetroX-TRE3G retroviral plasmid (Clontech). Src-MER and STAT3-MER were constructed by modifying the oestrogen receptor (MER, amino acids 281–599) and subcloning into the pCX4 plasmid. mCherry-CAAX was constructed using the C-terminal region of human KRAS (amino acids 166-189) and subcloning into the pCX4 plasmid. mCherry-GPI was also subcloned into the pCX4 plasmid (generously donated by Dr. Kiyokawa) (Yagi et al, 2012). All constructs were confirmed by sequencing. Gene transfer of pCX4 and pRrtroX-TRE3G was carried out by retroviral infection. Retroviral production and infection were performed as described previously (Kajiwara et al, 2014).

Surgical procedures of mice

Compensatory renal growth was induced by right UNX in male mice (8 weeks of age) under anesthesia as previously described (Chen et al, 2015). Renal growth was evaluated by measuring the weight of remaining kidney and the body. Left kidneys of sham-nephrectomised mice were used as controls for UNX mice.

Statistics and reproducibility

For data analyses, unpaired two-tailed *t*-tests were used to determine the *P*-values. For multiple group comparisons, two-way ANOVA was used. A *P*-value less than 0.05 was considered to be significant. All data and statistics were derived from at least three independent experiments.

Data availability

Supporting microarray data have been deposited in the Gene Expression Omnibus (GEO) under accession code GSE99375. All other supporting data are available from the corresponding author upon request.

Acknowledgments

We thank Dr. Yamano and Dr. Takata for consultation on experiments, Dr. Kiyokawa for providing the mCherry-GPI plasmid, Dr. Saito for mass spectrometry analysis and the Spectrography and Bioimaging Facility (NIBB Core Research Facilities). The inhibitor kit was provided by the Screening Committee of Anticancer Drugs supported by Grant-in-Aid for Scientific Research on Innovative Areas, Scientific Support Programs for Cancer Research, from The Ministry of Education, Culture, Sports, Science and Technology of Japan. This work was supported by Grant-in-Aid for Young Scientists (26830071, to K.K.), Grant-in-Aid for Scientific Research (C) (19K07639, to K.K.), Grant-in-Aid for Scientific Research (B) (19H03504, to M.O.), Grant-in-Aid for Scientific Research on Innovative Area (19H04962, to M.O.), Grant-in-Aid for Scientific Research on Innovative Area (16H01447, to K.A.) from the Ministry of Education, Culture, Sports and Technology of Japan to K.K.; the Takeda Science Foundation; the Extramural Collaborative Research Grant of Cancer Research Institute, Kanazawa University to K.K.

Author Contributions

K.K. designed study and performed most experiments and data analysis. K.A. carried out time-lapse imaging. D.O. performed microarray analysis. K.M. supported experiments. K.K. and M.O. wrote the manuscript with input from all authors.

Conflict of interest

The authors declare that they have no conflict of interest.

References

Adams MN, Harrington BS, He Y, Davies CM, Wallace SJ, Chetty NP, Crandon AJ, Oliveira NB, Shannon CM, Coward JI, Lumley JW, Perrin LC, Armes JE, Hooper JD (2015) EGF inhibits constitutive internalization and palmitoylation-dependent degradation of membrane-spanning procancer CDCP1 promoting its availability on the cell surface. *Oncogene* **34**: 1375-1383

Akagi T, Sasai K, Hanafusa H (2003) Refractory nature of normal human diploid fibroblasts with respect to oncogene-mediated transformation. *Proc Natl Acad Sci U S A* **100**: 13567-13572

Alajati A, Guccini I, Pinton S, Garcia-Escudero R, Bernasocchi T, Sarti M, Montani E, Rinaldi A, Montemurro F, Catapano C, Bertoni F, Alimonti A (2015) Interaction of CDCP1 with HER2 enhances HER2-driven tumorigenesis and promotes trastuzumab resistance in breast cancer. *Cell Rep* **11**: 564-576

Alvares SM, Dunn CA, Brown TA, Wayner EE, Carter WG (2008) The role of membrane microdomains in transmembrane signaling through the epithelial glycoprotein Gp140/CDCP1. *Biochim Biophys Acta* **1780**: 486-496

Anderson WA (1967) The fine structure of compensatory growth in the rat kidney after unilateral nephrectomy. *Am J Anat* **121**: 217-247

Awakura Y, Nakamura E, Takahashi T, Kotani H, Mikami Y, Kadowaki T, Myoumoto A, Akiyama H, Ito N, Kamoto T, Manabe T, Nobumasa H, Tsujimoto G, Ogawa O (2008) Microarray-based identification of CUB-domain containing protein 1 as a potential prognostic marker in conventional renal cell carcinoma. *J Cancer Res Clin Oncol* **134**: 1363-1369

Boccaccio C, Ando M, Tamagnone L, Bardelli A, Michieli P, Battistini C, Comoglio PM (1998) Induction of epithelial tubules by growth factor HGF depends on the STAT pathway. *Nature* **391**: 285-288

Bowes RC, 3rd, Lightfoot RT, Van De Water B, Stevens JL (1999) Hepatocyte growth factor induces tubulogenesis of primary renal proximal tubular epithelial cells. *J Cell Physiol* **180**: 81-90

Bromberg JF, Horvath CM, Besser D, Lathem WW, Darnell JE, Jr. (1998) Stat3 activation is required for cellular transformation by v-src. *Mol Cell Biol* **18**: 2553-2558

Casar B, He Y, Iconomou M, Hooper JD, Quigley JP, Deryugina EI (2012) Blocking of CDCP1 cleavage in vivo prevents Akt-dependent survival and inhibits metastatic colonization through PARP1-mediated apoptosis of cancer cells. *Oncogene* **31**: 3924-3938

Casar B, Rimann I, Kato H, Shattil SJ, Quigley JP, Deryugina EI (2014) In vivo cleaved CDCP1 promotes early tumor dissemination via complexing with activated beta1 integrin and induction of FAK/PI3K/Akt motility signaling. *Oncogene* **33**: 255-268
Chang-Panesso M, Humphreys BD (2017) Cellular plasticity in kidney injury and repair. *Nat Rev Nephrol* **13**: 39-46
Chen JK, Chen J, Neilson EG, Harris RC (2005) Role of mammalian target of rapamycin signaling in compensatory renal hypertrophy. *J Am Soc Nephrol* **16**: 1384-1391
Chen JK, Chen J, Thomas G, Kozma SC, Harris RC (2009) S6 kinase 1 knockout inhibits uninephrectomy- or diabetes-induced renal hypertrophy. *Am J Physiol Renal Physiol* **297**: F585-593
Chen JK, Nagai K, Chen J, Plieth D, Hino M, Xu J, Sha F, Ikizler TA, Quarles CC, Threadgill DW, Neilson EG, Harris RC (2015) Phosphatidylinositol 3-kinase signaling determines kidney size. *J Clin Invest* **125**: 2429-2444
Cheung KJ, Gabrielson E, Werb Z, Ewald AJ (2013) Collective invasion in breast cancer requires a conserved basal epithelial program. *Cell* **155**: 1639-1651
Date K, Matsumoto K, Shimura H, Tanaka M, Nakamura T (1997) HGF/NK4 is a specific antagonist for pleiotrophic actions of hepatocyte growth factor. *Febs Letters* **420**: 1-6
Dong Y, He Y, de Boer L, Stack MS, Lumley JW, Clements JA, Hooper JD (2012) The cell surface glycoprotein CUB domain-containing protein 1 (CDCP1) contributes to epidermal growth factor receptor-mediated cell migration. *J Biol Chem* **287**: 9792-9803
Emerling BM, Benes CH, Poulogiannis G, Bell EL, Courtney K, Liu H, Choo-Wing R, Bellinger G, Tsukazawa KS, Brown V, Signoretti S, Soltoff SP, Cantley LC (2013) Identification of CDCP1 as a hypoxia-inducible factor 2alpha (HIF-2alpha) target gene that is associated with survival in clear cell renal cell carcinoma patients. *Proc Natl Acad Sci U S A* **110**: 3483-3488
Fine L (1986) The biology of renal hypertrophy. *Kidney International* **29**: 619-634
Gao CF, Vande Woude GF (2005) HGF/SF-Met signaling in tumor progression. *Cell Res* **15**: 49-51
Gusenbauer S, Vlaicu P, Ullrich A (2013) HGF induces novel EGFR functions involved in resistance formation to tyrosine kinase inhibitors. *Oncogene* **32**: 3846-3856
Hammerman MR, O'Shea M, Miller SB (1993) Role of growth factors in regulation of renal growth. *Annu Rev Physiol* **55**: 305-321
He Y, Harrington BS, Hooper JD (2016) New crossroads for potential therapeutic intervention in cancer - intersections between CDCP1, EGFR family members and downstream signaling pathways. *Oncoscience* **3**: 5-8
Hooper JD, Zijlstra A, Aimes RT, Liang H, Claassen GF, Tarin D, Testa JE, Quigley JP (2003) Subtractive immunization using highly metastatic human tumor cells identifies SIMA135/CDCP1, a 135 kDa cell surface phosphorylated glycoprotein antigen. *Oncogene* **22**: 1783-1794
Ikeda J, Oda T, Inoue M, Uekita T, Sakai R, Okumura M, Aozasa K, Morii E (2009) Expression of CUB domain containing protein (CDCP1) is correlated with prognosis and survival of patients with adenocarcinoma of lung. *Cancer Sci* **100**: 429-433
Ishibashi K, Sasaki S, Sakamoto H, Hoshino Y, Nakamura T, Marumo F (1992) Expressions of receptor gene for hepatocyte growth factor in kidney after unilateral nephrectomy and renal injury. *Biochem Biophys Res Commun* **187**: 1454-1459
Joannidis M, Spokes K, Nakamura T, Faletto D, Cantley LG (1994) Regional expression of hepatocyte growth factor/c-met in experimental renal hypertrophy and hyperplasia. *Am J Physiol* **267**: F231-236
Kajiwara K, Yamada T, Bamba T, Fukusaki E, Imamoto F, Okada M, Oneyama C (2014) c-Src-induced activation of ceramide metabolism impairs membrane microdomains and promotes malignant progression by facilitating the translocation of c-Src to focal adhesions. *Biochem J* **458**: 81-93
Kermorgant S, Parker PJ (2008) Receptor trafficking controls weak signal delivery: a strategy used by c-Met for STAT3 nuclear accumulation. *J Cell Biol* **182**: 855-863
Khwaja A, Lehmann K, Marte BM, Downward J (1998) Phosphoinositide 3-kinase induces scattering and tubulogenesis in epithelial cells through a novel pathway. *J Biol Chem* **273**: 18793-18801

Kollmorgen G, Niederfellner G, Lifke A, Spohn GJ, Rieder N, Harring SV, Bauss F, Burtscher H, Lammers R, Bossenmaier B (2013) Antibody mediated CDCP1 degradation as mode of action for cancer targeted therapy. *Mol Oncol* **7**: 1142-1151

Kuroiwa M, Oneyama C, Nada S, Okada M (2011) The guanine nucleotide exchange factor Arhgef5 plays crucial roles in Src-induced podosome formation. *J Cell Sci* **124**: 1726-1738

Law ME, Corsino PE, Jahn SC, Davis BJ, Chen S, Patel B, Pham K, Lu J, Sheppard B, Norgaard P, Hong J, Higgins P, Kim JS, Luesch H, Law BK (2013) Glucocorticoids and histone deacetylase inhibitors cooperate to block the invasiveness of basal-like breast cancer cells through novel mechanisms. *Oncogene* **32**: 1316-1329

Law ME, Ferreira RB, Davis BJ, Higgins PJ, Kim JS, Castellano RK, Chen S, Luesch H, Law BK (2016) CUB domain-containing protein 1 and the epidermal growth factor receptor cooperate to induce cell detachment. *Breast Cancer Res* **18**: 80

Leroy C, Shen Q, Strande V, Meyer R, McLaughlin ME, Lezan E, Bentires-Alj M, Voshol H, Bonenfant D, Alex Gaither L (2015) CUB-domain-containing protein 1 overexpression in solid cancers promotes cancer cell growth by activating Src family kinases. *Oncogene* **34**: 5593-5598

Lin CY, Chen HJ, Huang CC, Lai LC, Lu TP, Tseng GC, Kuo TT, Kuok QY, Hsu JL, Sung SY, Hung MC, Sher YP (2014) ADAM9 promotes lung cancer metastases to brain by a plasminogen activator-based pathway. *Cancer Res* **74**: 5229-5243

Lindemans CA, Calafiore M, Mertelsmann AM, O'Connor MH, Dudakov JA, Jenq RR, Velardi E, Young LF, Smith OM, Lawrence G, Ivanov JA, Fu YY, Takashima S, Hua G, Martin ML, O'Rourke KP, Lo YH, Mokry M, Romera-Hernandez M, Cupedo T, Dow L, Nieuwenhuis EE, Shroyer NF, Liu C, Kolesnick R, van den Brink MRM, Hanash AM (2015) Interleukin-22 promotes intestinal-stem-cell-mediated epithelial regeneration. *Nature* **528**: 560-564

Liu H, Ong SE, Badu-Nkansah K, Schindler J, White FM, Hynes RO (2011) CUB-domain-containing protein 1 (CDCP1) activates Src to promote melanoma metastasis. *Proc Natl Acad Sci U S A* **108**: 1379-1384

Matsumoto K, Nakamura T (2001) Hepatocyte growth factor: renotropic role and potential therapeutics for renal diseases. *Kidney Int* **59**: 2023-2038

Miyazawa Y, Uekita T, Hiraoka N, Fujii S, Kosuge T, Kanai Y, Nojima Y, Sakai R (2010) CUB domain-containing protein 1, a prognostic factor for human pancreatic cancers, promotes cell migration and extracellular matrix degradation. *Cancer Res* **70**: 5136-5146

Montesano R, Matsumoto K, Nakamura T, Orci L (1991a) Identification of a fibroblast-derived epithelial morphogen as hepatocyte growth factor. *Cell* **67**: 901-908

Montesano R, Schaller G, Orci L (1991b) Induction of epithelial tubular morphogenesis in vitro by fibroblast-derived soluble factors. *Cell* **66**: 697-711

Nagaike M, Hirao S, Tajima H, Noji S, Taniguchi S, Matsumoto K, Nakamura T (1991) Renotropic functions of hepatocyte growth factor in renal regeneration after unilateral nephrectomy. *J Biol Chem* **266**: 22781-22784

Nakamura T, Sakai K, Nakamura T, Matsumoto K (2011) Hepatocyte growth factor twenty years on: Much more than a growth factor. *J Gastroenterol Hepatol* **26 Suppl 1**: 188-202

O'Brien LE, Tang K, Kats ES, Schutz-Geschwender A, Lipschutz JH, Mostov KE (2004) ERK and MMPs sequentially regulate distinct stages of epithelial tubule development. *Dev Cell* **7**: 21-32

O'Brien LE, Zegers MM, Mostov KE (2002) Opinion: Building epithelial architecture: insights from three-dimensional culture models. *Nat Rev Mol Cell Biol* **3**: 531-537

Oneyama C, Iino T, Saito K, Suzuki K, Ogawa A, Okada M (2009) Transforming potential of Src family kinases is limited by the cholesterol-enriched membrane microdomain. *Mol Cell Biol* **29**: 6462-6472

Pollack AL, Runyan RB, Mostov KE (1998) Morphogenetic mechanisms of epithelial tubulogenesis: MDCK cell polarity is transiently rearranged without loss of cell-cell contact during scatter factor/hepatocyte growth factor-induced tubulogenesis. *Dev Biol* **204**: 64-79

Santos OF, Moura LA, Rosen EM, Nigam SK (1993) Modulation of HGF-induced tubulogenesis and branching by multiple phosphorylation mechanisms. *Dev Biol* **159**: 535-548
Scherl-Mostageer M, Sommergruber W, Abseher R, Hauptmann R, Ambros P, Schweifer N (2001) Identification of a novel gene, CDCP1, overexpressed in human colorectal cancer. *Oncogene* **20**: 4402-4408
Spassov DS, Wong CH, Wong SY, Reiter JF, Moasser MM (2013) Trask loss enhances tumorigenic growth by liberating integrin signaling and growth factor receptor cross-talk in unanchored cells. *Cancer Res* **73**: 1168-1179
Tan RJ, Liu Y (2012) Matrix metalloproteinases in kidney homeostasis and diseases. *Am J Physiol Renal Physiol* **302**: F1351-1361
Taub R (2004) Liver regeneration: from myth to mechanism. *Nat Rev Mol Cell Biol* **5**: 836-847
Tierney MT, Aydogdu T, Sala D, Malecova B, Gatto S, Puri PL, Latella L, Sacco A (2014) STAT3 signaling controls satellite cell expansion and skeletal muscle repair. *Nat Med* **20**: 1182-1186
Trusolino L, Bertotti A, Comoglio PM (2010) MET signalling: principles and functions in development, organ regeneration and cancer. *Nat Rev Mol Cell Biol* **11**: 834-848
Turdo F, Bianchi F, Gasparini P, Sandri M, Sasso M, De Cecco L, Forte L, Casalini P, Aiello P, Sfondrini L, Agresti R, Carcangiu ML, Plantamura I, Sozzi G, Tagliabue E, Campiglio M (2016) CDCP1 is a novel marker of the most aggressive human triple-negative breast cancers. *Oncotarget* **7**: 69649-69665
Uekita T, Jia L, Narisawa-Saito M, Yokota J, Kiyono T, Sakai R (2007) CUB domain-containing protein 1 is a novel regulator of anoikis resistance in lung adenocarcinoma. *Mol Cell Biol* **27**: 7649-7660
Wortmann A, He Y, Christensen ME, Linn M, Lumley JW, Pollock PM, Waterhouse NJ, Hooper JD (2011) Cellular settings mediating Src Substrate switching between focal adhesion kinase tyrosine 861 and CUB-domain-containing protein 1 (CDCP1) tyrosine 734. *J Biol Chem* **286**: 42303-42315
Wortmann A, He Y, Deryugina EI, Quigley JP, Hooper JD (2009) The cell surface glycoprotein CDCP1 in cancer--insights, opportunities, and challenges. *IUBMB Life* **61**: 723-730
Wright HJ, Arulmoli J, Motazedi M, Nelson LJ, Heinemann FS, Flanagan LA, Razorenova OV (2016) CDCP1 cleavage is necessary for homodimerization-induced migration of triple-negative breast cancer. *Oncogene* **35**: 4762-4772
Yagi S, Matsuda M, Kiyokawa E (2012) Suppression of Rac1 activity at the apical membrane of MDCK cells is essential for cyst structure maintenance. *EMBO Rep* **13**: 237-243
Yu CL, Meyer DJ, Campbell GS, Larner AC, Carter-Su C, Schwartz J, Jove R (1995) Enhanced DNA-binding activity of a Stat3-related protein in cells transformed by the Src oncoprotein. *Science* **269**: 81-83
Yu H, Pardoll D, Jove R (2009) STATs in cancer inflammation and immunity: a leading role for STAT3. *Nat Rev Cancer* **9**: 798-809
Zegers MM (2014) 3D in vitro cell culture models of tube formation. *Semin Cell Dev Biol* **31**: 132-140

Figure legends

Figure 1. CDCP1 is required for HGF-induced phenotypic changes. (**A**) MDCK cysts embedded within the collagen matrix were pretreated with NK4 (1 μg/ml), Torin1 (+, 50 nM; ++, 100 nM), rapamycin (+ Rapa, 50 nM; ++ Rapa, 100 nM), or dasatinib (20 nM, Das), and then incubated in the presence of HGF (50 ng/ml) for one day. Ki67 was visualised with an Alexa Fluor 488-conjugated antibody (green), and actin filaments were stained with Alexa Fluor 594-phalloidin (magenta); arrowheads indicate transiently formed protrusions. (**B**) Diameter (μM) of cysts (n = 100). Dotted blue line indicates the average diameter of non-treated cysts. (**C**) Fraction of the total number of cysts counted (n > 100) with protrusions. (**D**) MDCK cysts embedded within the collagen matrix were incubated in the presence of HGF (50 ng/ml) for the indicated time periods. Activated Src (pY418) was visualised with an Alexa Fluor 488-conjugated antibody (green), and actin filaments were stained with Alexa Fluor 594-phalloidin (magenta); arrowheads indicate transiently formed protrusions. (**E**) mCherry-GPI-overexpressing MDCK cysts embedded within the collagen matrix were incubated in the presence of HGF (50 ng/ml) for the indicated time periods. Actin filaments were stained with Alexa Fluor 488-phalloidin (green). (**F**) MDCK cysts embedded within the collagen matrix were incubated in the presence of HGF (50 ng/ml) for the indicated time periods. Localisation of CDCP1 was visualised using an Alexa Fluor 488-conjugated antibody (green), and actin filaments were stained with Alexa Fluor 594-phalloidin (magenta). (**G**) Wild-type and CDCP1-knockout MDCK cysts were incubated in the presence of HGF (50 ng/ml) for 1 day. Ki67 was visualised with an Alexa Fluor 594-conjugated antibody (magenta), and actin filaments were stained with Alexa Fluor 488-phalloidin; arrowheads indicate transiently formed protrusions. Scale bars indicate 50 μm. (**H**) Diameter (μm) of cysts (n = 100). (**I**) Fraction of the total number of cysts counted (n > 100) with protrusions. Scale bars indicate 10 μm. The mean ratios ± SD were obtained from three independent experiments. **, $P < 0.01$; ***, $P < 0.001$; ****, $P < 0.0001$; NS, not significantly different; ANOVA was calculated compared to HGF-treated cysts.

Figure 2. Upregulation of CDCP1 induces HGF-related phenotypic changes by activating Src in lipid rafts. (**A**) Schematic of analysis of TRE-CDCP1-EGFP-harbouring MDCK cysts (CDCP1-EGFP cysts). TRE-CDCP1-EGFP-harbouring cells were cultured within a collagen matrix for 5 days for cyst formation, and then CDCP1-EGFP cysts were incubated in the presence of Dox for ~ 4 days. (**B**) CDCP1-EGFP cysts embedded within the collagen matrix were incubated in the presence of Dox (1 μg/ml) for the indicated time periods. Actin filaments were stained with Alexa Fluor 594-phalloidin (magenta). Arrowheads indicate protruding cells and open arrowheads indicate multi-layered structures. (**C**) CDCP1-EGFP cysts were incubated in the presence of Dox (1 μg/ml) for 2 days. Activated Src was visualised with a Src pY418 antibody (magenta). (**D**) CDCP1-EGFP cysts embedded within the collagen matrix were pretreated with 20 nM dasatinib for 2 h, and then incubated with Dox (1 μg/ml) for 4 days. (**E**) CDCP1-YF-EGFP and CDCP1-CG-EGFP cysts embedded within the collagen matrix were incubated in the presence of Dox (1 μg/ml) for 4 days. Actin filaments were stained with Alexa Fluor 594-phalloidin (magenta). Scale bars indicate 50 mm. (**F**) Fraction of the total number of cysts counted (n > 150) with protrusions. The mean ratios ± SD were obtained from three independent experiments. ***, $P < 0.001$; ****, $P < 0.0001$; NS, not significantly different; ANOVA compared to the Dox-treated cysts.

Figure 3. STAT3 activation is required for CDCP1-induced phenotypic changes. (**A**) CDCP1-myc- and mutant-overexpressing MDCK cells were embedded within the collagen matrix and cultured for 9 days. Cyst lysates were subjected to immunoblotting using the indicated antibodies. (**B**) CDCP1-EGFP cysts were incubated with Dox (1 μg/ml) for 2 or 4 days, and then subjected to quantitative real-time PCR. Relative mRNA expression levels were calculated by setting the mean value for non-treated cysts to one. The mean ratios ± SD were obtained from three independent experiments. ANOVA calculated compared to non-treated cysts. (C) CDCP1-EGFP cysts were pretreated with the indicated STAT3-specific inhibitors for 2 h and then incubated with Dox (1 μg/ml) for 4 days. Dotted blue indicates the average diameter of non-treated cysts. (**D**) STAT3-Y705F-overexpressing CDCP1-EGFP cysts were incubated with Dox (1 μg/ml) for 4 days. Actin filaments were stained with Alexa

Fluor 594-phalloidin (magenta). Scale bars indicate 50 μm. (e, f) MDCK cysts embedded within the collagen matrix were pretreated with S3i-201 (+ S3i, 50 nM; ++ S3i, 100 nM) or Stattic (+ Sta, 2.5 nM; ++ Sta, 5.0 nM) for 2 hours and incubated in the presence of HGF (50 ng/ml) for 1 day. (**E**) Diameter (μm) of cysts (n = 100). (**F**) Fraction of the total number of cysts counted (n > 100) with protrusions. The mean ratios ± SD were obtained from three independent experiments. *, $P < 0.05$; **, $P < 0.01$; ***, $P < 0.001$; ****, $P < 0.0001$; NS, not significantly different; ANOVA was calculated compared to the HGF-treated cysts.

Figure 4. CDCP1-Met association is required for CDCP1-induced phenotypic changes. (**A**) CDCP1-EGFP cysts were pretreated with the indicated Met-specific inhibitors for 2 h and then incubated with Dox (1 μg/ml) for 4 days. (**B**) Schematic representation of CDCP1 and the deletion mutants. SP, signal peptide; CUB, CUB domain; TM, transmembrane domain; CD, cytosolic domain. (**C**) Lysates from HEK293 cells overexpressing both CDCP1-myc and Met were subjected to immunoprecipitation with an anti-myc-tag antibody. Immunoprecipitates were subjected to immunoblotting using the indicated antibodies (IgG HC, IgG heavy chain). (**D**) CDCP1-myc- and CDCP1-PR-myc-overexpressing MDCK cells were embedded within the collagen matrix and cultured for 9 days. Cyst lysates were subjected to immunoblotting analysis using the indicated antibodies. (**E**) CDCP1-PR-EGFP cysts embedded within the collagen matrix were incubated with Dox (1 μg/ml) for 4 days. Actin filaments were stained with Alexa Fluor 594-phalloidin (magenta). Scale bars indicate 50 μm. (**F**) Fraction of the total number of cysts counted (n > 150) with protrusions. The mean ratios ± SD were obtained from three independent experiments. **, $P < 0.001$; ****, $P < 0.0001$; NS, not significantly different; ANOVA was calculated compared to the Dox-treated cysts. (**G**) Schematic model of the role of CDCP1-Met association in Src-induced STAT3 phosphorylation.

Figure 5. Compensatory renal growth after UNX is suppressed in *Cdcp1*-knockout mice. (**A**) *Cdcp1* wild-type (+/+), heterozygous (+/-), and homozygous knockout (-/-) mice at 8 weeks of age were subjected to left UNX or sham operation. Regenerative growth of remaining left kidney was analysed 8 weeks after operation and increases in remaining kidney/body weight ratios were assessed. (**B**) The mean ratios ± SD were obtained from ten mice per group. (**C**) The remaining kidney was removed from UNX- or sham-operated mice, and proximal tubules were stained with FITC-LTL (green). Scale bars indicate 50 mm. (**D**) Proximal tubules thickness was determined by the length of FITC-LTL-stained epithelial cell layer (n = 100). The mean ratios ± SD were obtained from five mice per group. *, $P < 0.05$; **, $P < 0.01$; ****, $P < 0.0001$; NS, not significantly different; two-way ANOVA.

Figure 6. Met-STAT3 signalling is attenuated in *Cdcp1*-knockout mice. (**A**) *Cdcp1* wild-type (+/+) and homozygous knockout (-/-) mice at 8 weeks of age were subjected to left UNX or sham operation. Regenerative growth of remaining left kidney was analysed at the indicated time points after operation and increases in remaining kidney/body weight ratios were assessed. The mean ratios ± SD were obtained from at least six mice per group. (**B-D**, **F**, **G**) The remaining kidney after UNX was subjected to microscopic immunofluorescence analysis with specific antibodies against Met pY1234-1235 (**B**), STAT3 pY705 (**C**), Ki67 (**D**), collagen IV (**F**), and MMP9 (**G**) and Alexa Fluor 594-conjugated secondary antibody (magenta). Proximal tubules were visualized by staining with FITC-LTL (green). Scale bars indicate 50 μm. Ki67-positive proximal tubules (%) were estimated by calculating the ratio of Ki67-stained tubules to the total number of tubules (n > 100) (**E**). The mean ratios ± SD were obtained from three mice per group. *, $P < 0.05$; **, $P < 0.01$; ****, $P < 0.0001$; NS, not significantly different; two-way ANOVA was calculated compared to sham operated control. (**H**) Schematic model of HGF-induced adaptive renal regeneration. CDCP1-Src regulates the Met-STAT3 signalling leading to compensatory renal growth through induction of ECM rearrangement and cell growth/proliferation.

Fig 1

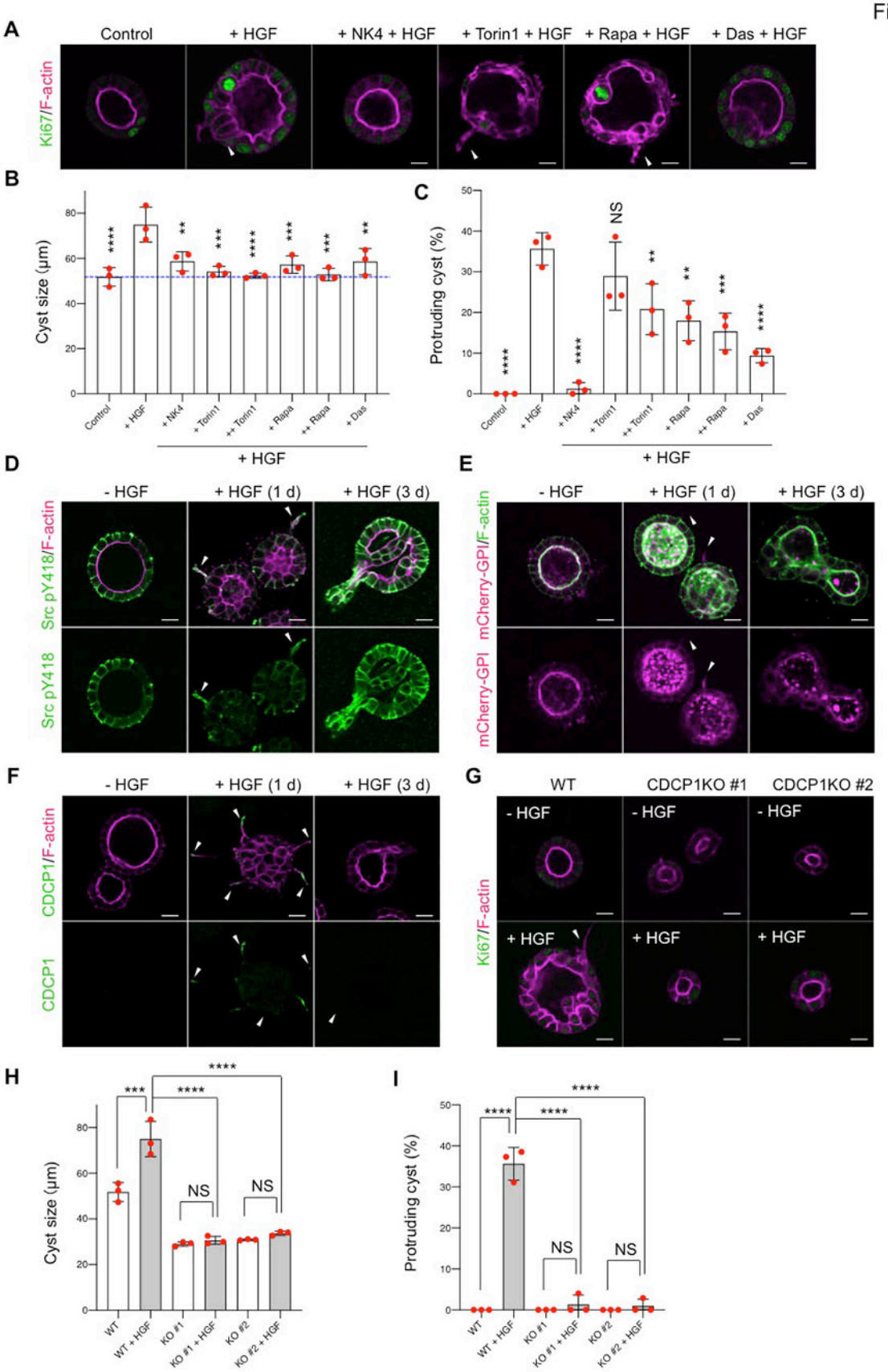
A
Control
+ HGF
+ NK4 + HGF
+ Torin1 + HGF
+ Rapa + HGF
+ Das + HGF
Ki67/F-actin
B
Cyst size (μm)
Control
+ HGF
+ NK4
+ Torin1
++ Torin1
+ Rapa
++ Rapa
+ Das
+ HGF
C
Protruding cyst (%)
NS
Control
+ HGF
+ NK4
+ Torin1
++ Torin1
+ Rapa
++ Rapa
+ Das
+ HGF
D
- HGF
+ HGF (1 d)
+ HGF (3 d)
Src pY418/F-actin
Src pY418
E
- HGF
+ HGF (1 d)
+ HGF (3 d)
mCherry-GPI/F-actin
mCherry-GPI
F
- HGF
+ HGF (1 d)
+ HGF (3 d)
CDCP1/F-actin
CDCP1
G
WT
CDCP1KO #1
CDCP1KO #2
- HGF
+ HGF
Ki67/F-actin
H
Cyst size (μm)
NS
NS
WT
WT + HGF
KO #1
KO #1 + HGF
KO #2
KO #2 + HGF
I
Protruding cyst (%)
NS
NS
WT
WT + HGF
KO #1
KO #1 + HGF
KO #2
KO #2 + HGF

Fig 2

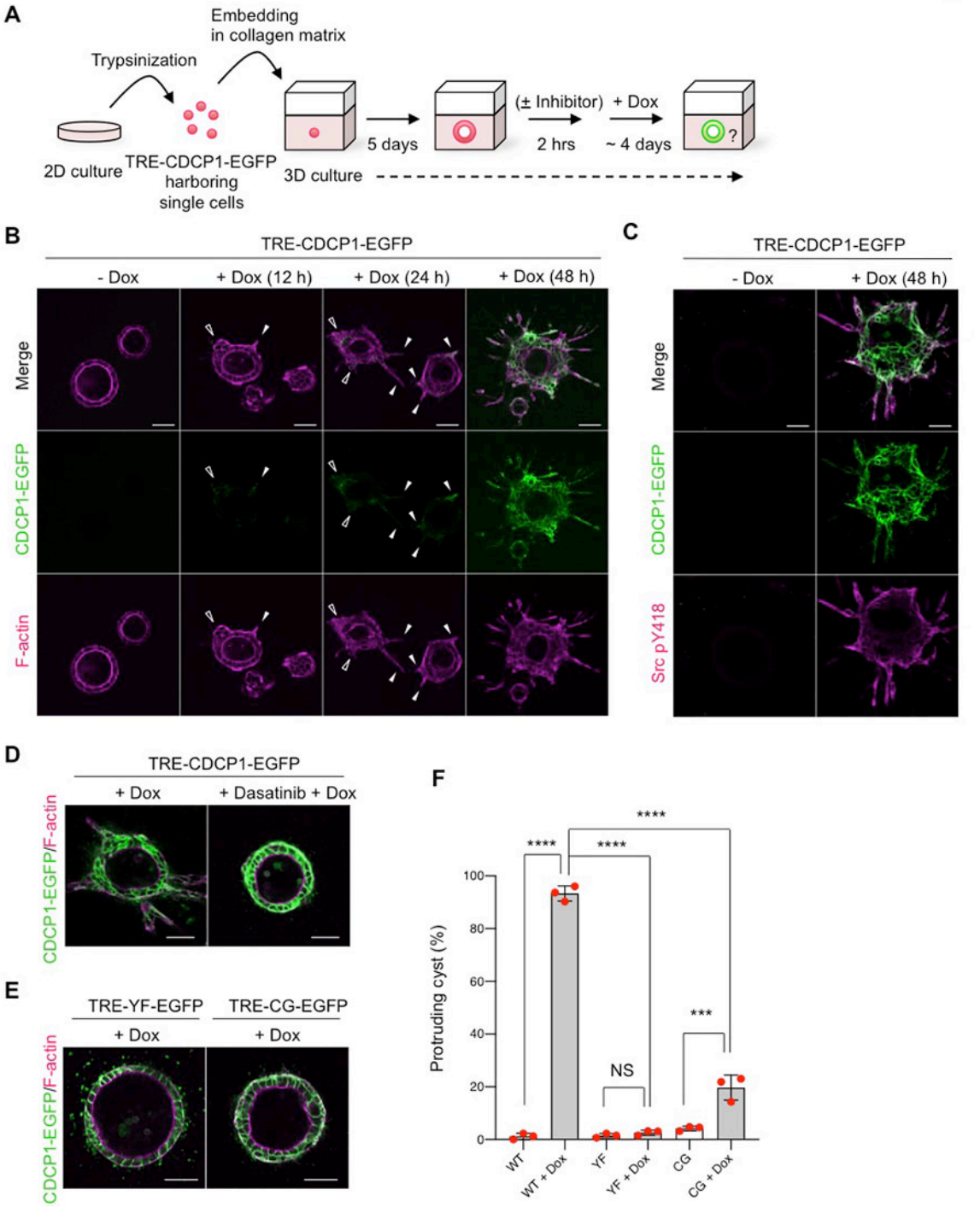
A
Embedding
in collagen matrix
Trypsinization
2D culture
TRE-CDCP1-EGFP
harboring
single cells
3D culture
5 days
(± Inhibitor)
2 hrs
+ Dox
~ 4 days
?
B
TRE-CDCP1-EGFP
- Dox
+ Dox (12 h)
+ Dox (24 h)
+ Dox (48 h)
Merge
CDCP1-EGFP
F-actin
C
TRE-CDCP1-EGFP
- Dox
+ Dox (48 h)
Merge
CDCP1-EGFP
Src pY418
D
TRE-CDCP1-EGFP
+ Dox
+ Dasatinib + Dox
CDCP1-EGFP/F-actin
E
TRE-YF-EGFP
TRE-CG-EGFP
+ Dox
+ Dox
CDCP1-EGFP/F-actin
F
Protruding cyst (%)
100
80
60
40
20
0
****
****
****
***
NS
WT
WT + Dox
YF
YF + Dox
CG
CG + Dox

Fig 3

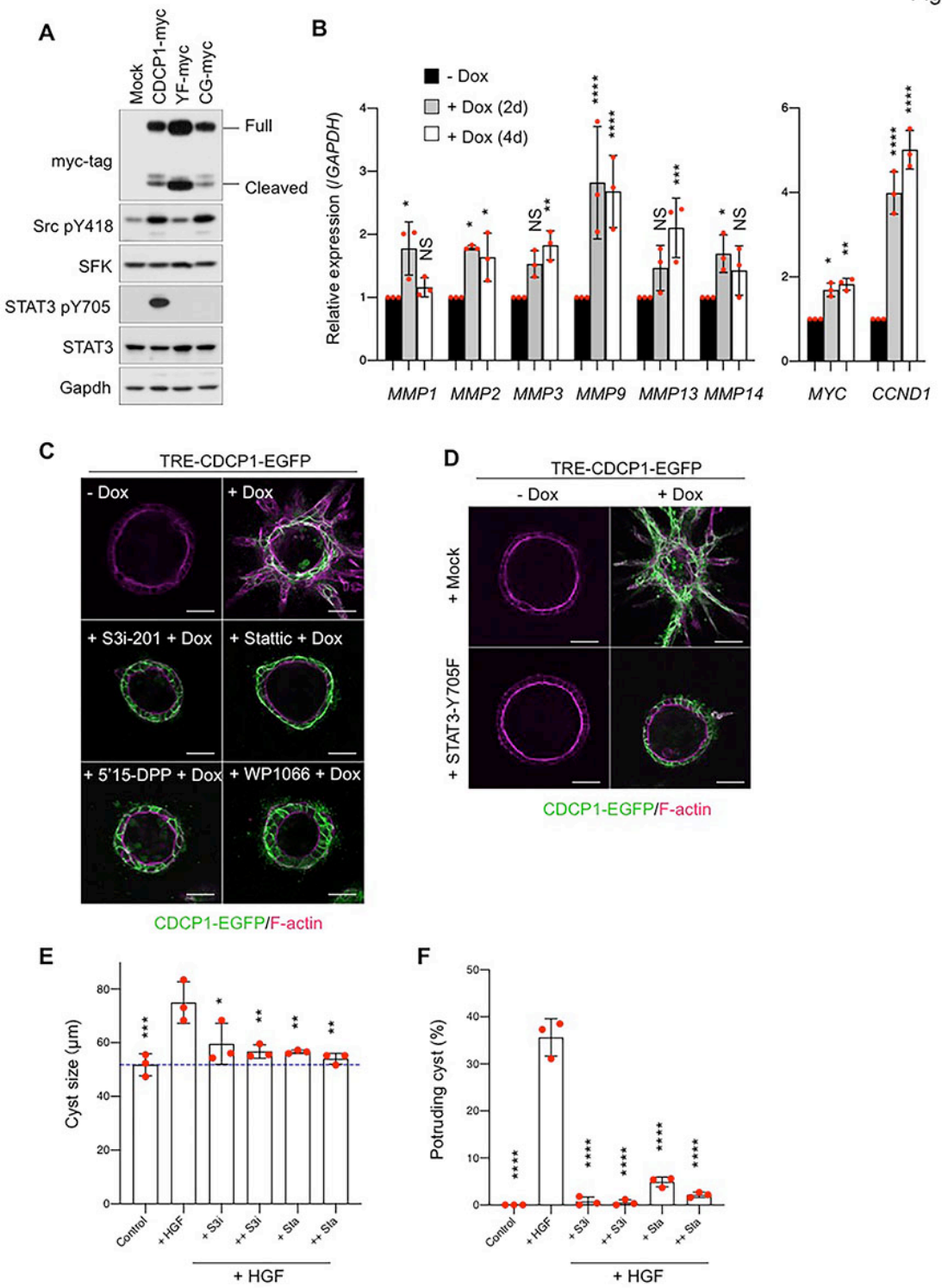
A
Mock
CDCP1-myc
YF-myc
CG-myc
myc-tag
Full
Cleaved
Src pY418
SFK
STAT3 pY705
STAT3
Gapdh
B
- Dox
+ Dox (2d)
+ Dox (4d)
Relative expression (/GAPDH)
MMP1
MMP2
MMP3
MMP9
MMP13
MMP14
MYC
CCND1
NS
C
TRE-CDCP1-EGFP
- Dox
+ Dox
+ S3i-201 + Dox
+ Stattic + Dox
+ 5'15-DPP + Dox
+ WP1066 + Dox
CDCP1-EGFP/F-actin
D
TRE-CDCP1-EGFP
- Dox
+ Dox
+ Mock
+ STAT3-Y705F
CDCP1-EGFP/F-actin
E
Cyst size (µm)
Control
+ HGF
+ S3i
++ S3i
+ Sta
++ Sta
+ HGF
F
Potruding cyst (%)
Control
+ HGF
+ S3i
++ S3i
+ Sta
++ Sta
+ HGF

Fig 4

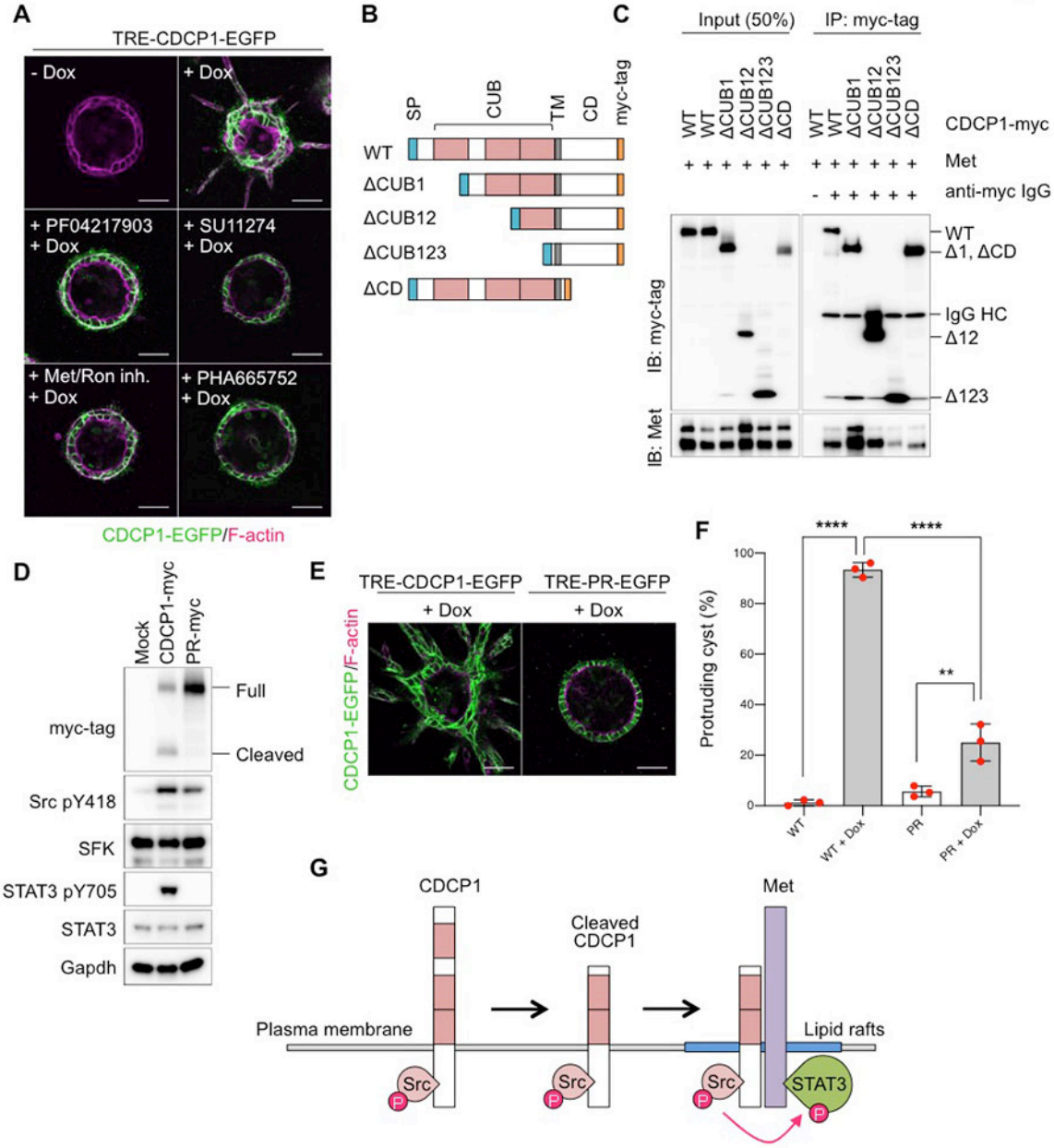
A
TRE-CDCP1-EGFP
- Dox
+ Dox
+ PF04217903 + Dox
+ SU11274 + Dox
+ Met/Ron inh. + Dox
+ PHA665752 + Dox
CDCP1-EGFP/F-actin
B
SP
CUB
TM
CD
myc-tag
WT
ΔCUB1
ΔCUB12
ΔCUB123
ΔCD
C
Input (50%)
IP: myc-tag
CDCP1-myc
Met
anti-myc IgG
IB: myc-tag
IB: Met
WT
Δ1, ΔCD
IgG HC
Δ12
Δ123
D
Mock
CDCP1-myc
PR-myc
Full
Cleaved
myc-tag
Src pY418
SFK
STAT3 pY705
STAT3
Gapdh
E
TRE-CDCP1-EGFP
TRE-PR-EGFP
+ Dox
CDCP1-EGFP/F-actin
F
Protruding cyst (%)
****
**
WT
WT + Dox
PR
PR + Dox
G
CDCP1
Cleaved CDCP1
Met
Plasma membrane
Lipid rafts
Src
STAT3
P

Fig 5

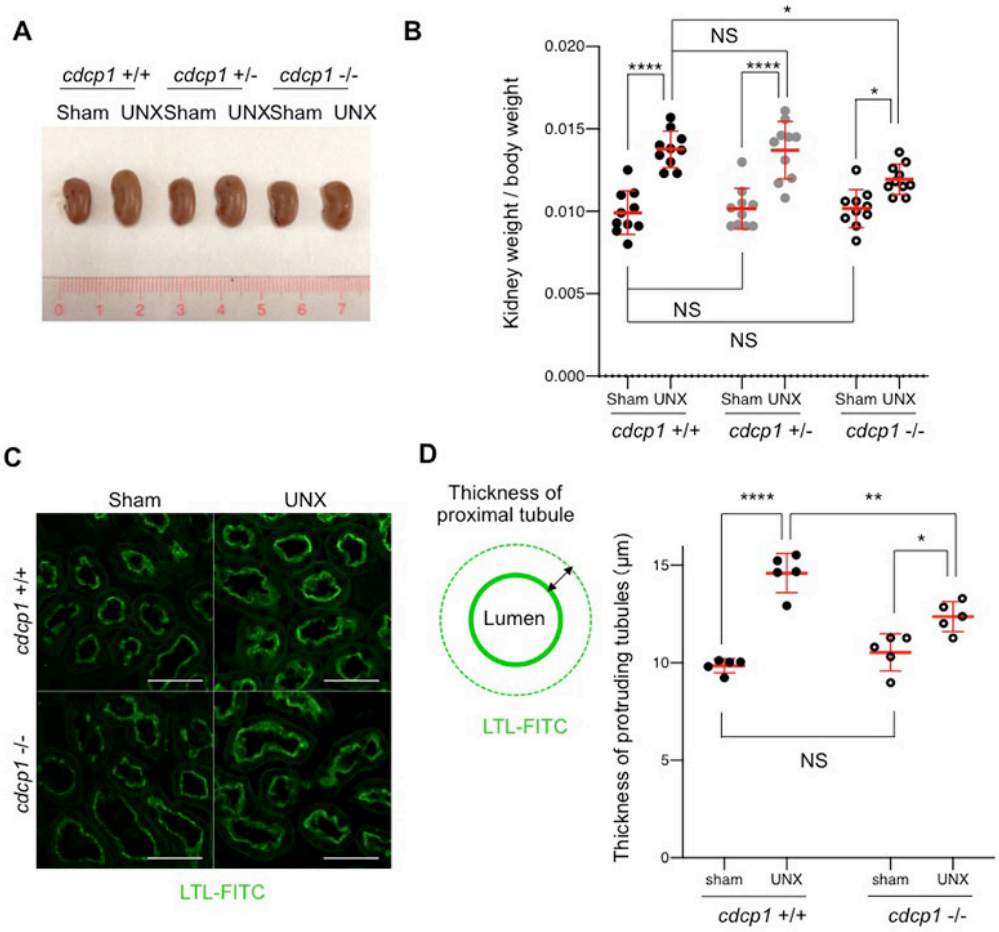
A
cdcp1 +/+
cdcp1 +/-
cdcp1 -/-
Sham UNX Sham UNX Sham UNX
B
Kidney weight / body weight
0.020
0.015
0.010
0.005
0.000
****
****
*
NS
NS
NS
Sham UNX
Sham UNX
Sham UNX
cdcp1 +/+
cdcp1 +/-
cdcp1 -/-
C
Sham
UNX
cdcp1 +/+
cdcp1 -/-
LTL-FITC
D
Thickness of proximal tubule
Lumen
LTL-FITC
Thickness of protruding tubules (μm)
15
10
5
0
****
**
*
NS
sham UNX
sham UNX
cdcp1 +/+
cdcp1 -/-

Fig 6

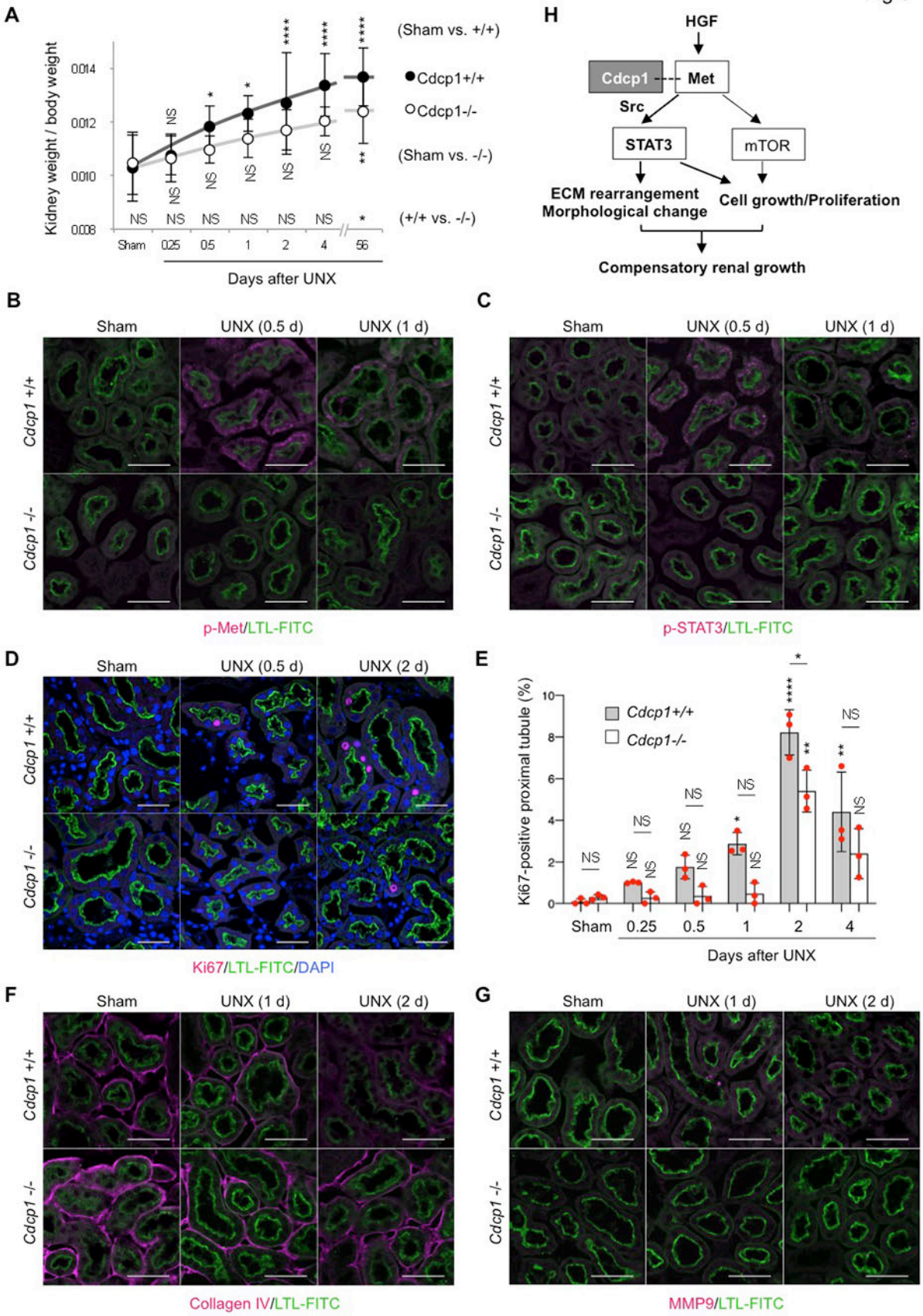
A
Kidney weight / body weight
0.014
0.012
0.010
0.008
Sham
0.25
0.5
1
2
4
56
Days after UNX
(Sham vs. +/+)
Cdcp1+/+
Cdcp1-/-
(Sham vs. -/-)
(+/+ vs. -/-)
NS
****
**
*
H
HGF
Cdcp1
Met
Src
STAT3
mTOR
ECM rearrangement
Morphological change
Cell growth/Proliferation
Compensatory renal growth
B
Sham
UNX (0.5 d)
UNX (1 d)
Cdcp1 +/+
Cdcp1 -/-
p-Met/LTL-FITC
C
p-STAT3/LTL-FITC
D
UNX (2 d)
Ki67/LTL-FITC/DAPI
E
Ki67-positive proximal tubule (%)
Cdcp1+/+
Cdcp1-/-
Days after UNX
F
Collagen IV/LTL-FITC
G
MMP9/LTL-FITC

Expanded View Figure legends

Fig EV1. Src associates with CDCP1 in lipid raft fractions. (**A**) Src-MER-overexpressing MDCK cells were incubated with 10 μM 4-OHT for the indicated time periods. Cell lysates were subjected to immunoblotting using the indicated antibodies. (**B**) Src-MER-overexpressing cysts embedded within the collagen matrix were incubated with 10 μM 4-OHT for 2 days. Activated Src was visualized with an anti-Src pY418 antibody (green). Actin filaments were stained with Alexa Fluor 594-phalloidin (magenta). Scale bars indicate 50 μm. (**C**) Src-MER-overexpressing MDCK cells were incubated with 10 μM 4-OHT for the indicated time periods. DRM and non-DRM fractions were separated in a sucrose density gradient. Aliquots of the fractions were subjected to immunoblotting analysis using an anti-Src pY418 antibody. **(D)** DRM fractions from Src-MER-activated cells were subjected to immunoprecipitation with an anti-oestrogen receptor (ERα) antibody. Immunoprecipitates were confirmed by silver staining. **(E)** Schematic flow diagram of identification of Src scaffolding proteins. All proteins within polyacrylamide gel were trypsinized and subjected to mass spectrometry. Proteins were identified using the SwissProt database and the number of identified proteins is depicted.

Fig EV2. Generation of CDCP1-knockout MDCK cells. (**A**) Schematic structure of CDCP1. In the cytoplasmic region, CDCP1 contains a Src association motif around Tyr734 and two palmitoylation sites (Cys residues 689 and 690), which are required for the localization of CDCP1 in lipid rafts. Upon phosphorylation at Tyr734 by Src, CDCP1 is additionally phosphorylated at Tyr762, resulting in direct association with PKCδ, which promotes cell migration. In the extracellular region, CDCP1 contains three CUB domains that are required for protein–protein interactions. CDCP1 also harbors a proteolytic cleavage (shedding) site between the first and second CUB domains and can, thus, be present in either the full-length or cleaved form depending on the cellular context. TM indicates transmembrane domain. (**B**) Schematic diagram of CRISPR/Cas9-based generation of CDCP1-knockout MDCK cells. Blue indicates the PAM sequence and bold letters indicate the start codon. The red arrowhead indicates the cleavage site. (**C**) Immunoblotting analysis of CDCP1-knockout MDCK cells. Lysates from wild-type and CDCP1-knockout MDCK cells were subjected to immunoblotting using the indicated antibodies. (**D**) CDCP1-knockout MDCK cysts were incubated in the presence of HGF (50 ng/ml) for 4 and 6 days. Ki67 was visualised with an Alexa Fluor 488-conjugated antibody (green) and actin filaments were stained with Alexa Fluor 594-phalloidin (magenta). Scale bars indicate 10 μm.

Fig EV2. Generation of CDCP1-knockout MDCK cells. (**A**) Schematic structure of CDCP1. In the cytoplasmic region, CDCP1 contains a Src association motif around Tyr734 and two palmitoylation sites (Cys residues 689 and 690), which are required for the localization of CDCP1 in lipid rafts. Upon phosphorylation at Tyr734 by Src, CDCP1 is additionally phosphorylated at Tyr762, resulting in direct association with PKCδ, which promotes cell migration. In the extracellular region, CDCP1 contains three CUB domains that are required for protein–protein interactions. CDCP1 also harbors a proteolytic cleavage (shedding) site between the first and second CUB domains and can, thus, be present in either the full-length or cleaved form depending on the cellular context. TM indicates transmembrane domain. (**B**) Schematic diagram of CRISPR/Cas9-based generation of CDCP1-knockout MDCK cells. Blue indicates the PAM sequence and bold letters indicate the start codon. The red arrowhead indicates the cleavage site. (**C**) Immunoblotting analysis of CDCP1-knockout MDCK cells. Lysates from wild-type and CDCP1-knockout MDCK cells were subjected to immunoblotting using the indicated antibodies. (**D**) CDCP1-knockout MDCK cysts were incubated in the presence of HGF (50 ng/ml) for 4 and 6 days. Ki67 was visualised with an Alexa Fluor 488-conjugated antibody (green) and actin filaments were stained with Alexa Fluor 594-phalloidin (magenta). Scale bars indicate 10 μm.

Fig EV3. CDCP1 recruits activated Src into lipid rafts. (**A**) TRE-CDCP1-EGFP (CDCP1-EGFP cells)- and mutant (YF-EGFP or CG-EGFP)-harboring MDCK cells were incubated in the presence of Dox (1 μg/ml) for the indicated time periods. Cell lysates were subjected to immunoblotting using the indicated antibodies. (**B**) CDCP1-EGFP cells were incubated in the

presence of Dox (1 μg/ml) for the indicated time periods. Actin filaments were stained with Alexa Fluor 594-phalloidin (magenta). Scale bars indicate 50 μm. (**C**) CDCP1-EGFP- and mutant-harboring MDCK cells were incubated in the presence of Dox (1 μg/ml) for 48 h. DRM and non-DRM fractions were separated on a sucrose density gradient. Aliquots of the fractions were subjected to immunoblotting analysis using the indicated antibodies. (**D**) DRM fractions of CDCP1-myc-overexpressing MDCK cells were subjected to immunoprecipitation with an anti-Src or anti-myc-tag antibody. Immunoprecipitates were subjected to immunoblotting using the indicated antibodies (IgG HC, and IgG heavy chain).

Fig EV4. Ingenuity Pathway Analysis of CDCP1-overexpressing cysts. (**A**) Gene ontology analysis of CDCP1-EGFP cysts. Magenta bars indicate signaling related to GO annotations. (**B**) STAT3 upstream regulatory networks of CDCP1-EGFP and CDCP1-CG-EGFP cysts. Activation Z-scores are presented in Supplementary Table 2. Red and green symbols indicate transcript levels upregulated and downregulated by CDCP1 overexpression, respectively. Arrows indicate activation (orange), inhibition (blue), inconsistency with the state of the downstream molecule (yellow) and unknown effect (grey). (**C**) Heat map representing changes in the expression of STAT3 target genes in CDCP1-EGFP (WT) and CDCP1-CG-EGFP (CG) cysts.

Fig EV5. Extracellular environments are altered by CDCP1 overexpression. (**A**) CDCP1-EGFP cysts embedded within the collagen matrix were incubated with Dox (1 μg/ml) for the indicated time periods. The basement membrane was visualized with an anti-laminin antibody (magenta). The arrowheads indicate protruding cells, and the open arrowheads indicate multi-layered structures. (**B**) CDCP1-EGFP cysts were pretreated with 20 μM marimastat for 2 h, and then incubated with Dox (1 μg/ml) for 4 days. The basement membrane was visualized using an anti-laminin antibody (magenta). (**C**) The histogram depicting the percentage of cells with protrusions was calculated by setting the total number of cysts to 100% (n > 150). (**D**) TRE-CDCP1-mCherry-harbouring MDCK cells were embedded within a 2% DQ-collagen-containing matrix. CDCP1-mCherry cysts were pretreated with 20 μM marimastat for 2 h, and then incubated with Dox (1 μg/ml) for 4 days. DQ fluorescence (green) was visualized under a fluorescent microscope. Scale bars indicate 50 μm. (**E, F**) MDCK cysts embedded within the collagen matrix were pretreated with marimastat (+ Mari, 10 μM; ++ Mari, 20 μM) for 2 hours, and then incubated in the presence of HGF (50 ng/ml) for 1 day. (**E**) Diameter of cysts (μm) of cysts (n = 100). Dotted blue line indicates the average diameter of non-treated cysts. (**F**) Fraction of the total number of cysts counted (n > 100). The mean ratios ± SD were obtained from three independent experiments. *, $P < 0.05$; **, $P < 0.01$; **** $P < 0.0001$, Two-way ANOVA was calculated relative to the HGF-treated cysts. (**G**) STAT3-MER-overexpressing cysts embedded within the collagen matrix were incubated with 1 μM 4-OHT for 4 days. STAT3-MER was visualized with ERα antibody (green) and actin filaments were stained with Alexa Fluor 594-phalloidin (magenta). Scale bars indicate 50 μm.

Fig EV6. Met-induced morphological changes are inhibited by CDCP1 knockout. (**A**) Wild-type and CDCP1-knockout TRE-Met harboring MDCK cells embedded within the collagen matrix were incubated with HGF (50 ng/ml) or Dox (1 μg/ml) for 4 days. Met was visualized with a Met antibody (green). (**B**) A schematic model of the role of CDCP1-Src in HGF-induced invasive growth. CDCP1-Src activates the Met-STAT3 signalling on lipid rafts, leading to invasive growth through induction of ECM rearrangement and cell growth/proliferation. The mTOR pathway also contributes to cell growth.

Fig EV7. Generation of *Cdcp1*-knockout mouse. (**A**) Schematic diagram of CRISPR/Cas9-based generation of *Cdcp1*-knockout mouse. Blue indicates the PAM sequence and bold letters indicate the start codon. The red arrowhead indicates the cleavage site. (**B**) PCR verification of deletion at 1st exon of *Cdcp1* gene using Fwd and Rev primers depicted in panel (A). (**C**) Representative picture of wild-type (+/+), *Cdcp1* heterozygous (+/-) and homozygous knockout (-/-) littermate mice at 8 weeks of age. (**D, E**) Whole body (**D**) and left kidney (**E**) weight of wild-type (+/+) and *Cdcp1* homozygous knockout (-/-) mice at 8 weeks of age. The mean ratios ± SD were obtained from ten mice per group. NS, not significantly different; unpaired two-tailed *t*-test.

Fig EV8. Met–STAT3 signaling is attenuated in *Cdcp1*-knockout mouse. (**A**) The remaining kidney of wild-type (+/+) and *Cdcp1* homozygous knockout (-/-) mice after UNX was subjected to immunofluorescence microscopic analysis using specific antibodies against CDCP1 pY734 and Alexa Fluor 594-conjugated secondary antibody (magenta). (**B-D**) The remaining kidney of wild-type (*Cdcp1* +/+) mice after UNX was subjected to immunofluorescence microscopic analysis using specific antibodies against Met pY1234-1235 (**B**), STAT3 pY705 (**C**), and Src pY418 (**D**) and Alexa Fluor 488-conjugated secondary antibody (green). Endosome marker EEA1 was visualized using Alexa Fluor 594-conjugated secondary antibody (magenta). (**E**) The remaining kidney of *Cdcp1* wild-type (+/+) and *Cdcp1* homozygous knockout (-/-) mice after UNX was subjected to immunofluorescence microscopic analysis using specific antibodies against MMP2 and Alexa Fluor 594-conjugated secondary antibody (magenta). Proximal tubules were visualized by staining with FITC-LTL (green). Scale bars indicate 50 μm. (**F**) Schematic diagram of changes in cellular events during compensatory renal growth of wild-type (+/+) and *Cdcp1* homozygous knockout (-/-) mice.

Fig EV9. Effects of CDCP1 expression on the morphology of MDCK cysts. (**A**) Downregulation of CDCP1 induces formation of a luminal structure. CDCP1-EGFP cysts embedded within the collagen matrix were incubated in the presence of Dox (1 μg/ml) for 4 days. Cysts were then incubated for an additional 5 days in the absence of Dox. (**B**) Upregulation of CDCP1 induces an expression of Cytokeratin 14. TRE-CDCP1-EGFP-harbouring cysts were incubated with Dox (1 μg/ml) for 4 days. Cytokeratin 14 (CK14) was visualized with a specific antibody (magenta). Scale bars indicate 50 μm.

Movie EV1. CDCP1 induced cell protrusion. CDCP1-EGFP MDCK cysts harboring mCherry-CAAX embedded within collagen matrix were incubated in the presence of Dox (1 μg/ml). Time-lapse images were captured at 30 min intervals for 40 h.

Dataset EV1. Upstream regulator analysis in Ingenuity Pathway Analysis.

Expanded View Tables

Table EV1 (part 1). Inhibitor screening for CDCP1-induced phenotypic changes in MDCK cysts

		Inhibiting effect	
Target	Compound	Protrusion formation	Multilayer construction
Met	PF-04217903	+++	+++
Met	SU11274	++	++
Met	PHA-665752	++	++
Met	Met/Ron inhibitor	++	++
Fms	GW2580	+	+
Flt-3	Flt-3 Inhibitor	-	-
EGFR/Her2	Lapatinib	-	-
EGFR	Gefitinib	-	-
EGFR	Erlotinib	-	-
VEGFR	VEGFR2 kinase inhibitor I	-	-
PDGFR	SU11652	-	-
IGF-IR	AGL 2263	-	-
IGF-IR	OSI-906	-	-
FGFR	PD173074	-	-
TGFb-R	LY2157299	-	-
Src	Dasatinib	+++	+++
STAT3	5,15-DPP	+++	++
STAT3	WP1066	++	++
STAT3	S3i-201	++	++
STAT3	Stattic	++	++
MEK	U-0126	+	+
PI3K	LY-294002	-	++
Akt	AKT inhibitor	+	+
Akt	Akt Inhibitor IV	+	+
Akt	Akt Inhibitor VIII	+	+
Akt	Akt Inhibitor XI	+	+
PKC	Go6983	-	-
Rac	Rac1 inhibitor	+	+
Rho/SRF	CCG-1423	-	-
ROCK	H-1152	-	-
ROCK	Y-27632	-	-
MLCK	ML-7	-	-

+++	Inhibition
++ / +	Weak inhibition
-	No inhibition

Table EV1 (part 2). Inhibitor screening for CDCP1-induced phenotypic changes in MDCK cysts

		Inhibiting effect	
Target	Compound	Protrusion formation	Multilayer construction
JAK	Ruxolitinib	-	-
JAK	Jak inhibitor I	-	-
GSK-3	TWS119	-	-
GSK-3	CT99021	-	-
HIF	Chetomin	++	++
HIF-PH	Dimethyloxalylglycine	-	-
Notch	DAPT	+	+
Wnt	IWR-1-endo	-	-
Hedgehog	Vismodegib	-	-
Aurora	MLN8237	+++	++
Aurora	ENMD-2076	+++	++
CDK	Alsterpaullone, 2-cyanoethyl	+	-
CDK	Cdk1/2 inhibitor III	+	-
CDK	NU6102	-	-
CDK	Kenpaullone	-	-
CDK	Cdk2/9 inhibitor	+	-
CDK	Purvalanol A	-	-
CDK	Olomoucine	+	-
CDK	Cdk4 inhibitor	+	+
CDK	3-ATA	+	-
ALK	A83-01	++	++
ALK	LDN193189	+	+
CCR2	RS 102895	-	-
CCR3	SB 328437	-	-
CXCR2	SB 225002	-	-
CXCR4	AMD3100 octahydrochloride	-	-
Tpl2	Tpl2 kinase inhibitor	-	-
MMP	Marimastat	+++	-
mTOR	Rapamycin	-	+++
mTOR	Temsirolimus	-	+++
mTOR	Everolimus	-	+++
mTOR	Torin1	-	+++
PDK1	OSU-03012	-	-
AMPK	Compound C	-	-

+++	Inhibition
++ / +	Weak inhibition
-	No inhibition

Table EV2. Sequences of quantitative RT-PCR

Gene	Forward primer (5'-3')	Reverse primer (5'-3')
GAPDH	gattgtcagcaatgcctcct	ggtcatggatgactttggcta
MMP1	gcaaatgcaggcgttctt	agattcagggtgtccgtgtc
MMP2	gacagccctgcaagttcc	ccgtggtacagctgtcgtag
MMP3	tgcagttagagatcacggagac	gggtaggcatgacccaaaa
MMP9	acggccgactatgacacc	ccgtcctgggtgtagagtttc
MMP13	gattcttctggcgattgcat	cggccaaaaggattttgtta
MMP14	ctcgccccagtcattctc	acgcgcagaccatagaactt
MYC	tgccaaaaggtccgaatc	ctgtgaggaggtttgctgtg
CCND1	gacgaactgctgcaaatgg	gtcatggctgccaggttc

Table EV3. Sequences of gRNAs and genotyping primers

Genes	gRNA (5'-3')
Canis CDCP1	ggcgccgccgagccat
Mus musculus Cdcp1	tgagaacccgcaggccgagt

Gene	Forward primer (5'-3')	Reverse primer (5'-3')
Mus musculus Cdcp1	gagtcatggcccactcggcctg	cctcctaaggcttgttccgcgc

Fig EV1

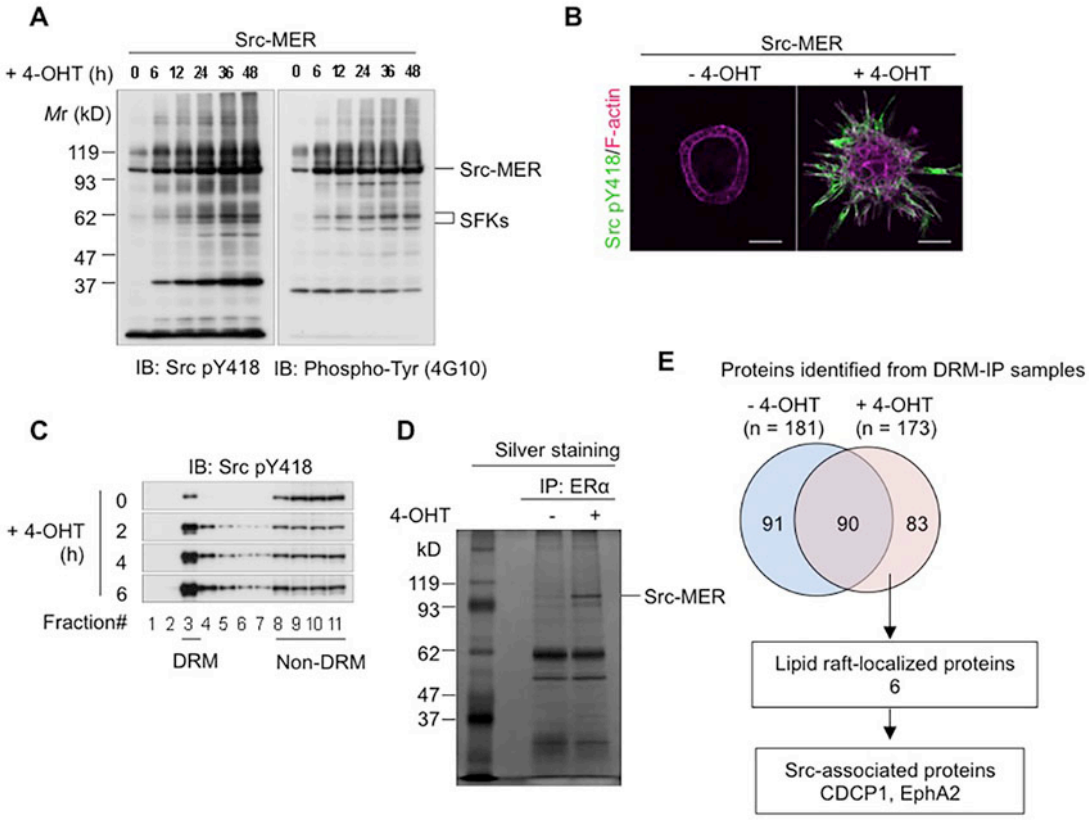
A
Src-MER
+ 4-OHT (h)
0 6 12 24 36 48
0 6 12 24 36 48
Mr (kD)
119
93
62
47
37
Src-MER
SFKs
IB: Src pY418
IB: Phospho-Tyr (4G10)
B
Src-MER
- 4-OHT
+ 4-OHT
Src pY418/F-actin
C
IB: Src pY418
+ 4-OHT (h)
0
2
4
6
Fraction#
1 2 3 4 5 6 7 8 9 10 11
DRM
Non-DRM
D
Silver staining
IP: ERα
4-OHT
-
+
kD
119
93
62
47
37
Src-MER
E
Proteins identified from DRM-IP samples
- 4-OHT (n = 181)
+ 4-OHT (n = 173)
91
90
83
Lipid raft-localized proteins
6
Src-associated proteins
CDCP1, EphA2

Fig EV2

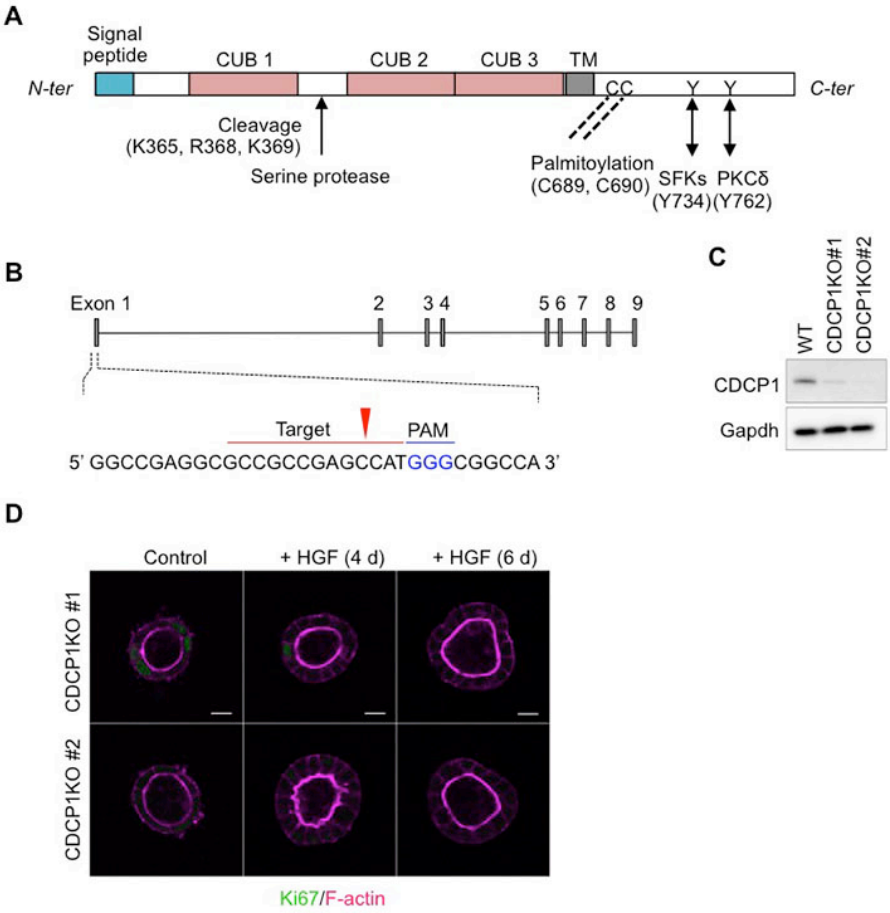
A
Signal peptide
CUB 1
CUB 2
CUB 3
TM
N-ter
CC
Y
Y
C-ter
Cleavage (K365, R368, K369)
Serine protease
Palmitoylation (C689, C690)
SFKs (Y734)
PKCδ (Y762)
B
Exon 1
2
3 4
5 6 7 8 9
Target
PAM
5' GGCCGAGGCGCCGCCGAGCCATGGGCGGCCA 3'
C
WT
CDCP1KO#1
CDCP1KO#2
CDCP1
Gapdh
D
Control
+ HGF (4 d)
+ HGF (6 d)
CDCP1KO #1
CDCP1KO #2
Ki67/F-actin

Fig EV3

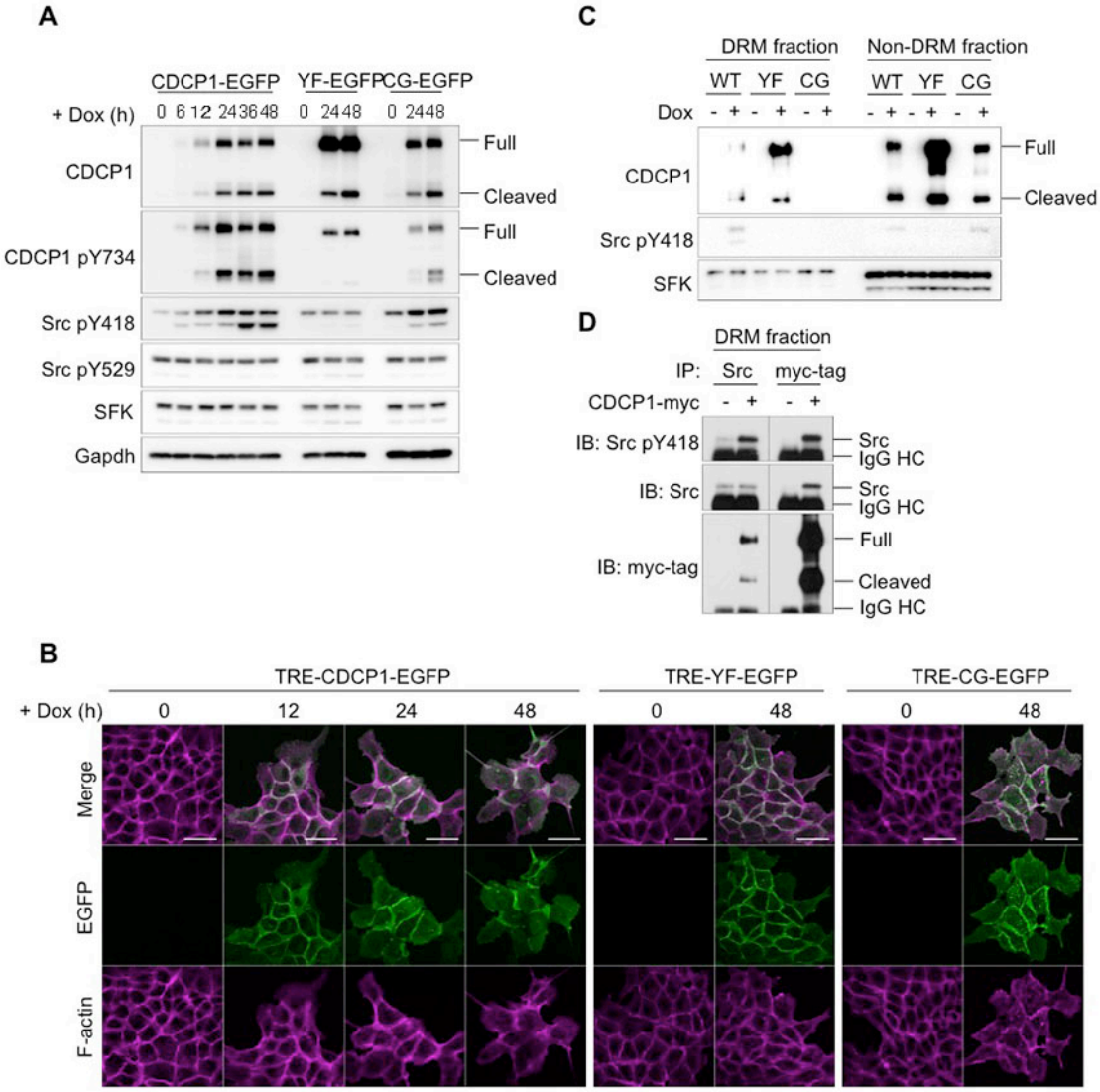
A
CDCP1-EGFP
YF-EGFP
CG-EGFP
+ Dox (h)
0 6 12 24 36 48
0 24 48
0 24 48
CDCP1
CDCP1 pY734
Src pY418
Src pY529
SFK
Gapdh
Full
Cleaved
Full
Cleaved
C
DRM fraction
Non-DRM fraction
WT
YF
CG
WT
YF
CG
Dox
CDCP1
Src pY418
SFK
Full
Cleaved
D
DRM fraction
IP:
Src
myc-tag
CDCP1-myc
IB: Src pY418
IB: Src
IB: myc-tag
Src
IgG HC
Src
IgG HC
Full
Cleaved
IgG HC
B
TRE-CDCP1-EGFP
TRE-YF-EGFP
TRE-CG-EGFP
+ Dox (h)
0
12
24
48
0
48
0
48
Merge
EGFP
F-actin

Fig EV4

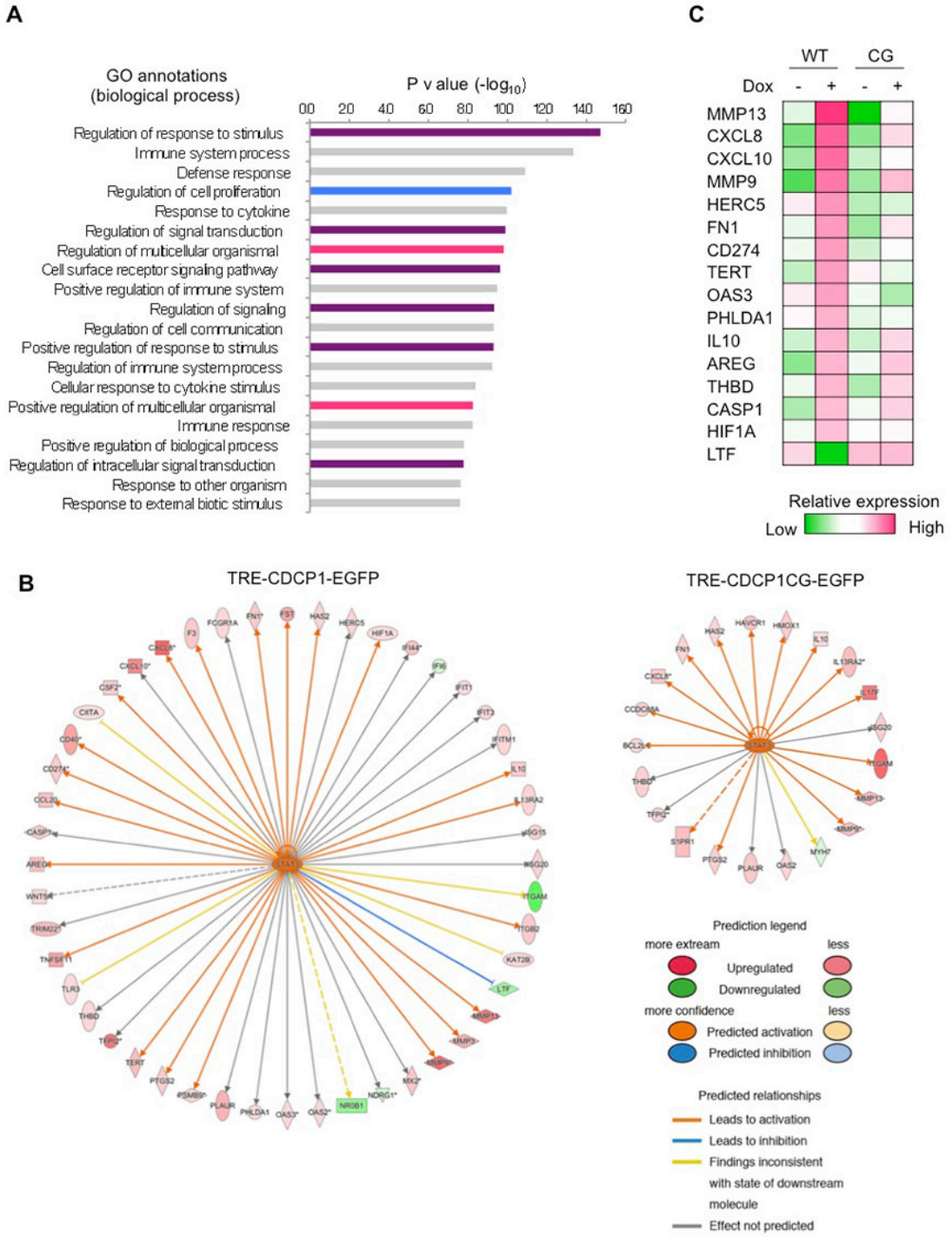
A
GO annotations
(biological process)
P value (-log10)
0.0 2.0 4.0 6.0 8.0 10.0 12.0 14.0 16.0
Regulation of response to stimulus
Immune system process
Defense response
Regulation of cell proliferation
Response to cytokine
Regulation of signal transduction
Regulation of multicellular organismal
Cell surface receptor signaling pathway
Positive regulation of immune system
Regulation of signaling
Regulation of cell communication
Positive regulation of response to stimulus
Regulation of immune system process
Cellular response to cytokine stimulus
Positive regulation of multicellular organismal
Immune response
Positive regulation of biological process
Regulation of intracellular signal transduction
Response to other organism
Response to external biotic stimulus
C
WT
CG
Dox
- + - +
MMP13
CXCL8
CXCL10
MMP9
HERC5
FN1
CD274
TERT
OAS3
PHLDA1
IL10
AREG
THBD
CASP1
HIF1A
LTF
Relative expression
Low
High
B
TRE-CDCP1-EGFP
TRE-CDCP1CG-EGFP
Prediction legend
more extream
less
Upregulated
Downregulated
more confidence
less
Predicted activation
Predicted inhibition
Predicted relationships
Leads to activation
Leads to inhibition
Findings inconsistent
with state of downstream
molecule
Effect not predicted

Fig EV5

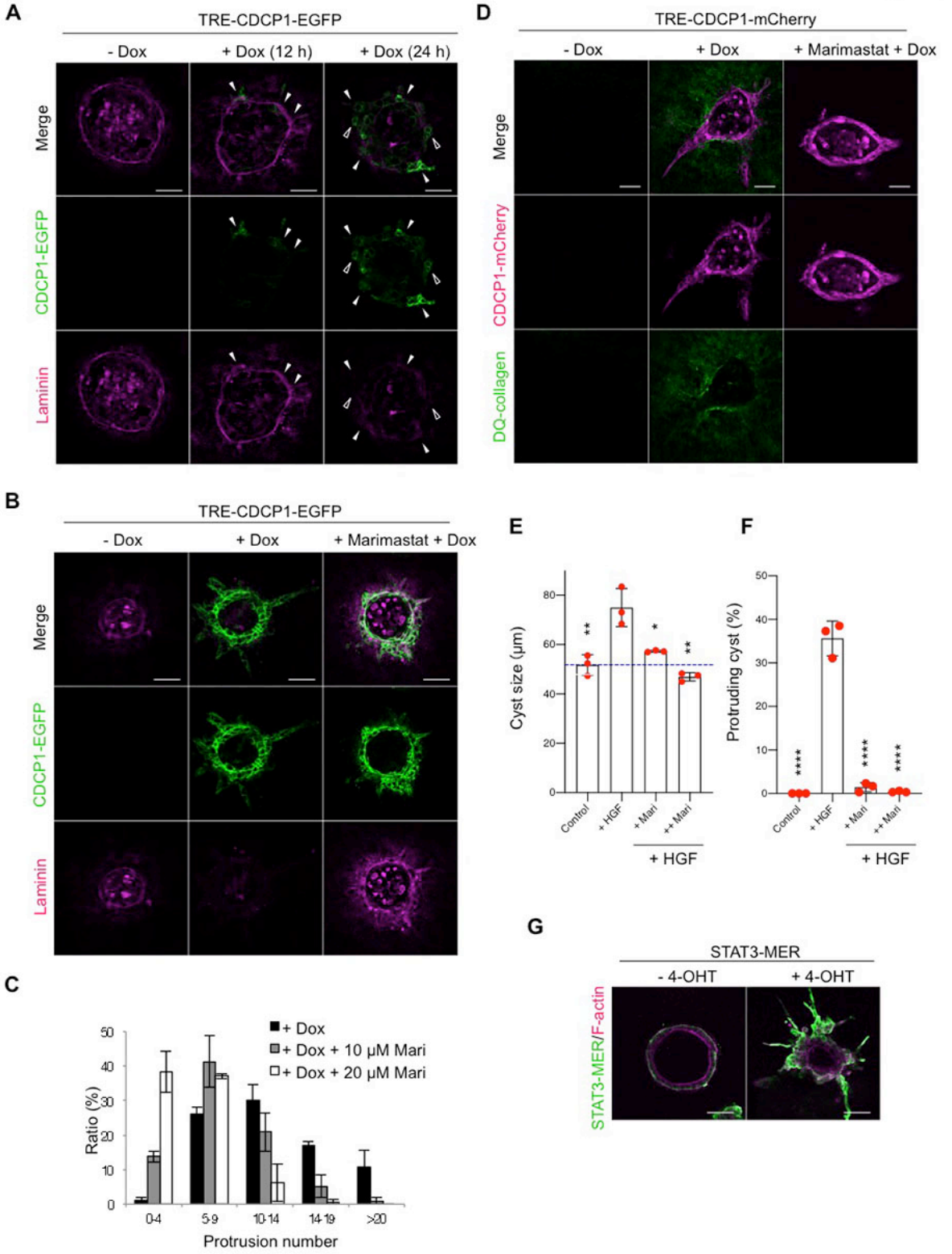
A
TRE-CDCP1-EGFP
- Dox
+ Dox (12 h)
+ Dox (24 h)
Merge
CDCP1-EGFP
Laminin
D
TRE-CDCP1-mCherry
- Dox
+ Dox
+ Marimastat + Dox
Merge
CDCP1-mCherry
DQ-collagen
B
TRE-CDCP1-EGFP
- Dox
+ Dox
+ Marimastat + Dox
Merge
CDCP1-EGFP
Laminin
E
Cyst size (µm)
Control
+ HGF
+ Mari
++ Mari
+ HGF
F
Protruding cyst (%)
Control
+ HGF
+ Mari
++ Mari
+ HGF
C
+ Dox
+ Dox + 10 µM Mari
+ Dox + 20 µM Mari
Ratio (%)
0-4
5-9
10-14
14-19
>20
Protrusion number
G
STAT3-MER
- 4-OHT
+ 4-OHT
STAT3-MER/F-actin

Fig EV6

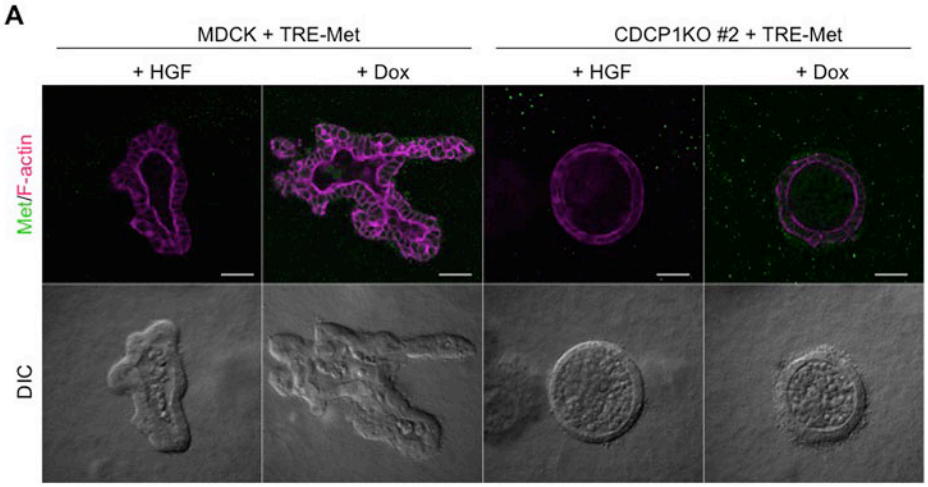
A
MDCK + TRE-Met
CDCP1KO #2 + TRE-Met
+ HGF
+ Dox
+ HGF
+ Dox
Met/F-actin
DIC

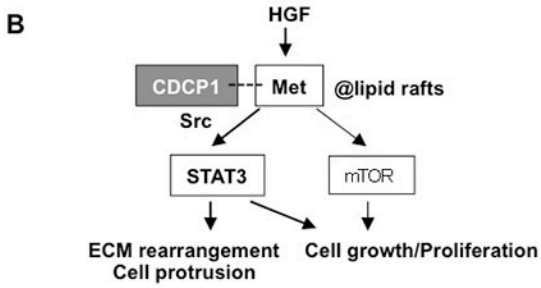
B
HGF
CDCP1
Met
@lipid rafts
Src
STAT3
mTOR
ECM rearrangement
Cell protrusion
Cell growth/Proliferation

Fig EV7

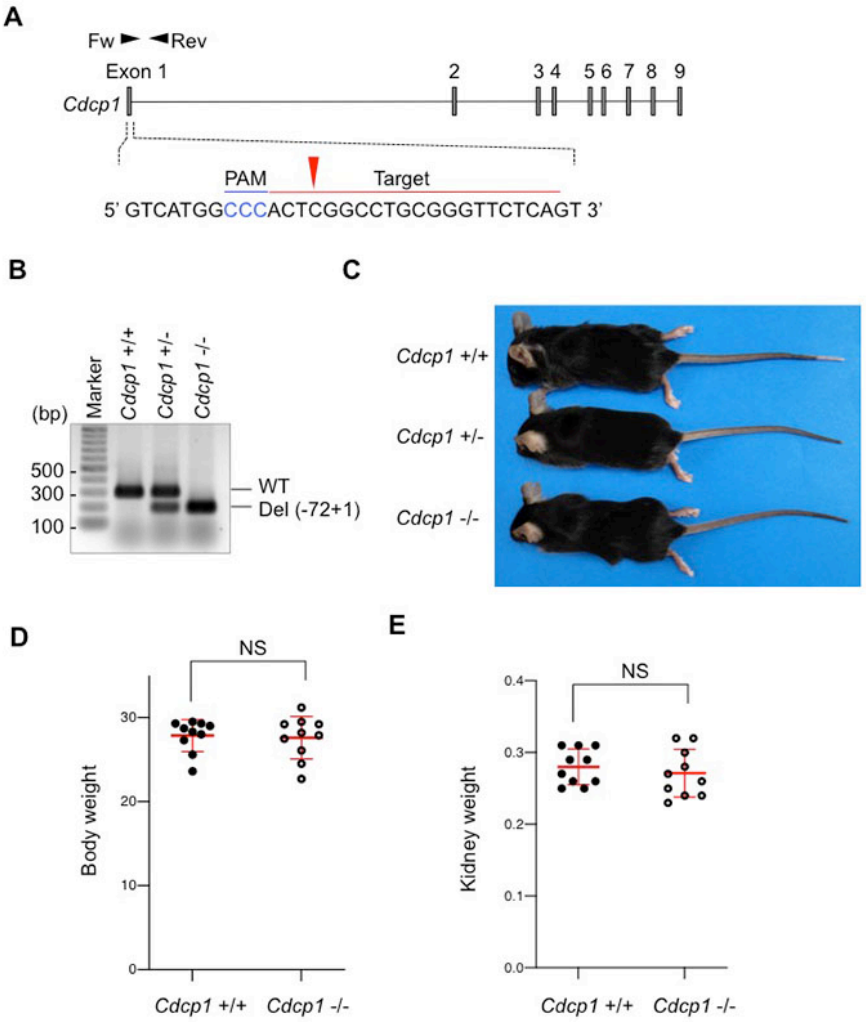
A
Fw
Rev
Exon 1
2
3 4
5 6
7
8
9
Cdcp1
PAM
Target
5' GTCATGGCCCACTCGGCCTGCGGGTTCTCAGT 3'
B
Marker
Cdcp1 +/+
Cdcp1 +/-
Cdcp1 -/-
(bp)
500
300
100
WT
Del (-72+1)
C
Cdcp1 +/+
Cdcp1 +/-
Cdcp1 -/-
D
NS
Body weight
30
20
10
0
Cdcp1 +/+
Cdcp1 -/-
E
NS
Kidney weight
0.4
0.3
0.2
0.1
0.0
Cdcp1 +/+
Cdcp1 -/-

Fig EV8

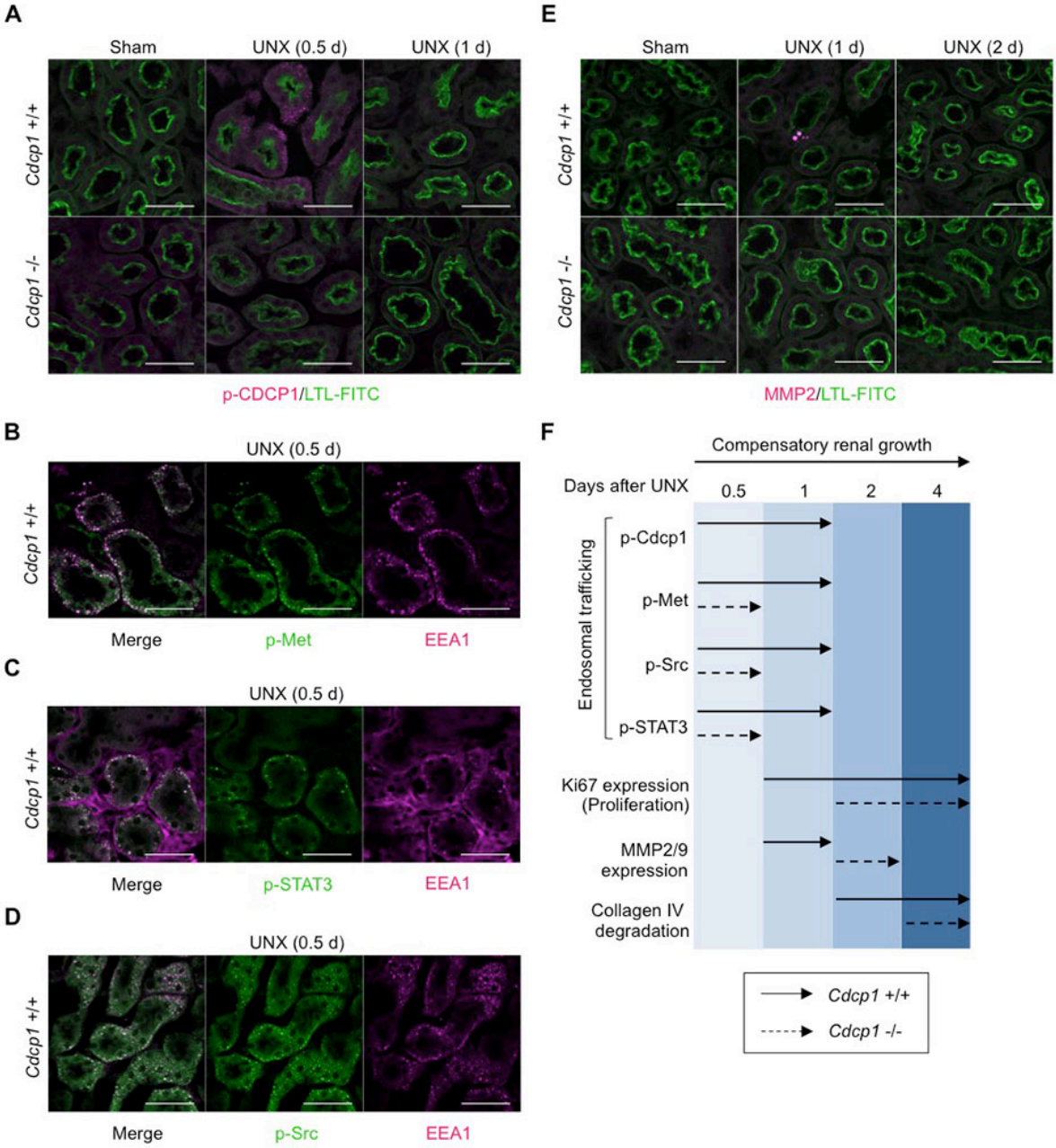
A
Sham
UNX (0.5 d)
UNX (1 d)
Cdcp1 +/+
Cdcp1 -/-
p-CDCP1/LTL-FITC
E
Sham
UNX (1 d)
UNX (2 d)
Cdcp1 +/+
Cdcp1 -/-
MMP2/LTL-FITC
B
UNX (0.5 d)
Cdcp1 +/+
Merge
p-Met
EEA1
C
UNX (0.5 d)
Cdcp1 +/+
Merge
p-STAT3
EEA1
D
UNX (0.5 d)
Cdcp1 +/+
Merge
p-Src
EEA1
F
Compensatory renal growth
Days after UNX
0.5
1
2
4
Endosomal trafficking
p-Cdcp1
p-Met
p-Src
p-STAT3
Ki67 expression
(Proliferation)
MMP2/9
expression
Collagen IV
degradation
Cdcp1 +/+
Cdcp1 -/-

Fig EV9

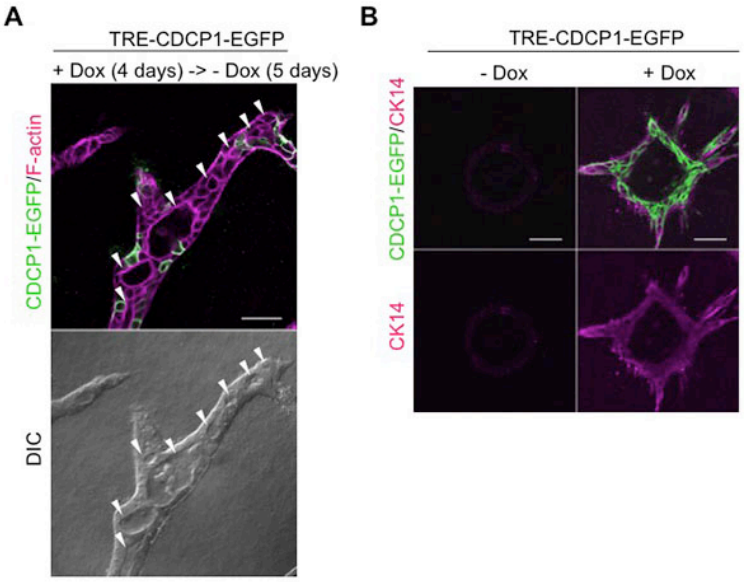
A
TRE-CDCP1-EGFP
+ Dox (4 days) -> - Dox (5 days)
CDCP1-EGFP/F-actin
DIC
B
TRE-CDCP1-EGFP
- Dox
+ Dox
CDCP1-EGFP/CK14
CK14